Stockholm University

Master Thesis

Degree Project in
Geology 45 hp

Hydrogeology of the Húsavik-Hafralækur area, northeast Iceland, and its link to earthquake related hydrogeochemical changes

Jenny Söderlindh

Stockholm 2019

Department of Geological Sciences
Stockholm University
SE-106 91 Stockholm

Hydrogeology of the Húsavik-Hafralækur area, northeast Iceland, and its link to earthquake related hydrogeochemical changes

Jenny Söderlindh

Title Page: View over Hafralækur and the wells HA-01 and HA-04

Abstract

This hydrogeological study shows that the groundwater in the Húsavik-Hafralækur area, northern Iceland, consists of three different water types with distinctly different isotopic and chemical signatures: modern meteoric water, pre-Holocene meteoric water and seawater located in aquifers close to each other, thereby providing excellent preconditions for hydrochemical earthquake monitoring. Hydrochemical changes have been observed in boreholes at Húsavik (HU-01) and Hafralækur (HA-01) prior to major (M > 5) earthquakes in 2012 and 2013. Those changes have been attributed to water mixing and/or water-rock interaction, but the water types that are proposed to mix and their geographic locations are poorly constrained. Therefore, in this study, the hydrogeology of the Húsavik-Hafralækur area was mapped for the purpose of identifying different water types and their sources. This was done by using stable isotopes (δ^2H and $\delta^{18}O$), conservative elements (Cl and B), and a suite of parameters (SiO_2, Na, K, Mg, Fe, Al, SO_4, F, Mn, Br, Mo, Sr, Ti, P, Li, CO_2, pH, and T) in water samples collected from boreholes, springs, streams, rivers and lakes (n = 41). The results show that (1) Ice Age waters (δ^2H < - 128 to - 122 ‰) are hot, equilibrated with Icelandic basalt, originate from deeper aquifers and emerge in lowland areas. (2) Modern meteoric waters (δ^2H < - 92 to - 58 ‰) are cold, not equilibrated with basalt and cover the whole area in shallow aquifers and surface waters. (3) Seawater infiltrates the bedrock at depth at the coast. (4) The monitored wells (HU-01 and HA-01) are fed by Ice Age aquifers flowing into the wells from below and/or from the sides, and the HU-01 well also receives a ~ 10 % seawater component. Because Ice Age water and modern meteoric water sources are located so near to one another, it is inferred that cracking of the wall rock, for example due to dilatational tectonic stresses prior to earthquakes, may cause mixing of these water components even at small strain rates.

Table of Contents

1. Introduction

Groundwater chemistry has been monitored in two boreholes in northern Iceland since 2002 (Húsavik, HU-01) (Claesson et al., 2007, 2004) and 2008 (HU-01 and Hafralækur, HA-01) (Andrén et al., 2016; Skelton et al., 2019, 2014; Wästeby et al., 2014). The 17 and 11-year long time series show changes in groundwater chemistry four to six months before earthquakes of magnitude (M) > 5 occurred (Andrén et al., 2016; Skelton et al., 2019, 2014). Since the monitoring started, this has happened twice (2012 and 2013) and has enabled statistical evaluation of the data, showing that the groundwater changes are probably associated with the earthquakes (Andrén et al., 2016; Skelton et al., 2019, 2014). Based on these findings, change in groundwater chemistry has been proposed as a possible earthquake precursor signal (Skelton et al., 2014). This is in accordance with other studies, where variations in stable isotope ratios (Reddy and Nagabhushanam, 2012), dissolved elements (Reddy and Nagabhushanam, 2012; Tsunogai and Wakita, 1995), and radon count rates (Einarsson et al., 2008; Igarashi et al., 1995) have been observed prior to earthquakes. Other proposed hydrological precursors include change in water levels in boreholes (e.g. Roeloffs, 1988).

The findings made at HU-01 (N66°03.323', W017°21.086') and HA-01 (N65°52.351', W017°27.154') have been made possible because of the radically different isotopic and chemical compositions of the groundwater sources that are mixing in this area, i.e. old Ice Age water seems to have mixed with present-day meteoric water.

Apart from water mixing, some of the hydrochemical changes at HU-01 and HA-01 have been attributed to water-rock interaction (Andrén et al., 2016; Claesson et al., 2007; Skelton et al., 2019, 2014; Wästeby et al., 2014). Water-rock interaction changes the groundwater chemistry by fracture induced increase in the reactive surface area of the rock, allowing water to react quickly with the rock (Scholz et al., 1973; Thomas, 1988).

The hydrochemical changes have occurred at very low estimated strains at both sites (Skelton et al., 2019), but the pre-seismic changes are contradictory: At Hafralækur, present-day meteoric water from a shallow source above seems to have flown into the well (Skelton et al., 2014), whereas at Húsavik, fluids from a deep (possible mantle) source below may have flowed into the well (Claesson et al., 2004).

These contradicting findings makes it challenging to understand the underlying cause of the changes. This is important because understanding coupling between groundwater chemical changes and earthquakes might make it possible to forecast them.

Dilatational pre-seismic strain has been proposed to account for both water mixing and water-rock interaction at HA-01 (Skelton et al., 2019, 2014) in accordance with the dilatancy model (Scholz et al., 1973). According to this model, a zone of cracked rocks is formed in the region of a future earthquake epicentre due to crustal stretching (Scholz et al., 1973). It has been proposed

that water then can flow down into the newly opened fractures and pores from the surrounding rock volume (Chi-Yuen Wang and Manga, 2010; Dobrovolsky et al., 1979; Scholz et al., 1973). This model has been used to explain other pre-seismic observations, such as falling groundwater levels (e.g. Kissin and Grinevsky, 1990; Roeloffs, 1988; Wang et al., 2018), and changes in seismic body-wave velocities due to a higher ratio of air filled pore spaces prior to earthquakes (Whitcomb et al., 1973). Since the estimated strain rate at HA-01 is so low, water transport has been proposed to occur in microfractures, which requires that the water sources are located only a short distance apart for mixing to be possible (Skelton et al., 2019).

The rising fluids proposed to be involved in pre-seismic hydrochemical changes at HU-01 (Claesson et al., 2004) are not as easily explained with the dilatancy model (Scholz et al., 1973). According to another model, Icelandic earthquakes are proposed to be caused by fluids rising from below, originating from a low-resistivity layer at around 15 km depth (Stefánsson, 2011). The rising fluids are proposed to cause sliding along deeply located fault planes and migrate upwards with time (Stefánsson, 2011). The process is proposed to be driven by the interplay between the Icelandic drift across the Mid Atlantic Ridge (MAR) and the stresses caused by the upwelling of mantle material from the hot spot plume under Iceland (Stefánsson, 2011; Stefánsson and Halldórsson, 1988). Observations of fluids at high fluid pressures that migrate upwards from the bottom of the seismogenic zone in the seismically active Húsavik-Flatey Fault (HFF) (Crampin et al., 2002), and measurements of fracture networks in the HFF indicating that vertical fluid transport is favoured before horizontal flow in the fault (Gudmundsson et al., 2001) support this model.

A full understanding of the causes of groundwater chemical changes associated with earthquakes requires detailed knowledge of the hydrology of the area. It is necessary to know which water types that are mixing in those wells and if the water flows into the wells from above, from below or from the sides. Today, little is known about the hydrogeology in the area and the locations and sources of the waters surrounding the wells.

The aim of this project is therefore to map the hydrogeology of the Húsavik-Hafralækur area and construct a conceptual hydrogeological model. The study will be conducted by collecting and analysing groundwater samples from wells, springs, rivers, streams and lakes in the Húsavik-Hafralækur area to identify different water types, their source(s) and to explore mixing between them. The purpose is to further our understanding of how earthquakes influence hydrogeology.

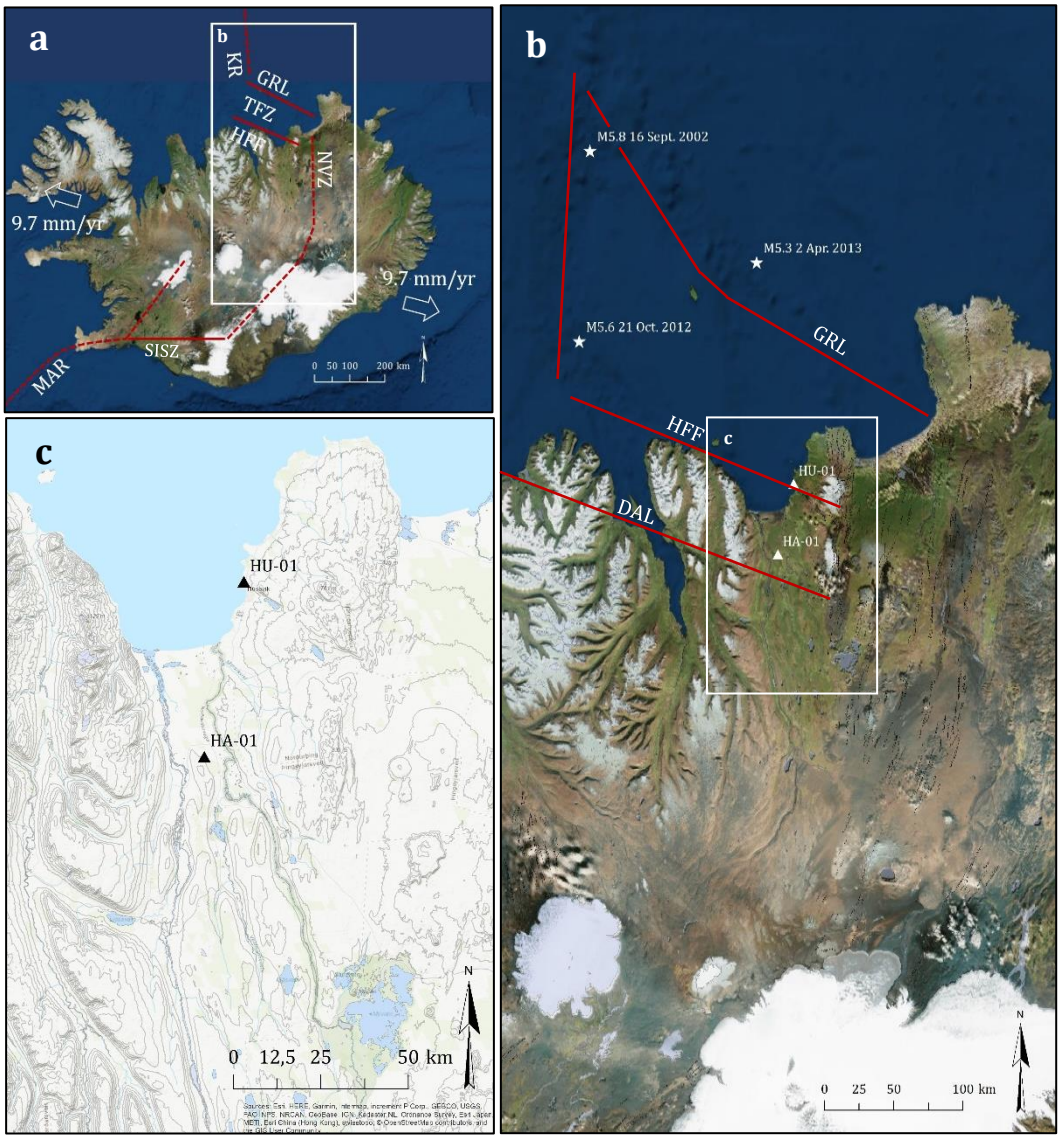

Figure 1. a) Tectonic map of Iceland showing the Mid Atlantic Ridge (MAR), Northern Volcanic Zone (NVZ), Tjörnes Fracture Zone (TFZ), Kolbeinsey Ridge (KR), Grímsey Lineament (GRL), and the Húsavík-Flatey Fault (HFF). The inset shows the location for **b)** the three M > 5 earthquakes that caused the hydrochemical changes at the boreholes in Húsavik (HU-01) and Hafralækur (HA-01), both marked on the map. The locations and magnitudes for the earthquakes on 16 September 2002 (M 5.8), 21 October 2012 (M 5.6), and 2 April 2013 (M 5.3) are from the global centroid moment tensor project (https://www.globalcmt.org/). The GRL, the HFF and the Dalvik Lineament (DAL) are shown by red lines. The map also shows the area from the coast to the glacier Vatnajökull, which is the recharge area for the river Skjálfandafljót west of HA-01. The inset shows **c)** a topographic map of the study area including the locations for the monitored boreholes HU-01 and HA-01. Each topographic line represents 100 m.

2. Background

2.1. Tectonic setting

Iceland is located on the Mid Atlantic Ridge and the spreading centre is expressed onshore (Fig. 1 a). A hotspot located under Vatnajökull has shifted the onshore expression of the MAR eastwards and has created two transform fault zones as a cause of this shift: the Tjörnes Fracture Zone (TFZ) in northern Iceland and the South Iceland Seismic Zone (SISZ) in southern Iceland. The approximate seafloor spreading velocity is 1.9 cm/yr and the spreading direction is 107 – 287 ˚ in the north and 103 – 283 ˚ in the south.

The study area is located within the TFZ, which is an oblique transform fault zone that connects the onshore NVZ with the offshore Kolbeinsey Ridge (KR), both of which are expressions of the MAR (Gudmundsson et al., 1993; Mariotto et al., 2014; Garcia and Dhont, 2005). The TFZ is about 120 km long from north to south and about 80 km wide from east to west (Gudmundsson et al., 1993; Garcia and Dhont, 2005) and comprises three parallel WNW-ESE striking main faults: the Grimsey Lineament (GRL), the HFF, and the Dalvik Lineament (DAL) (Gudmundsson et al., 1993; Mariotto et al., 2014; Garcia and Dhont, 2005) (Fig. 1 b). The TFZ is characterized by earthquakes with up to magnitude (M) 7 and the seismicity is mainly located within these active structures (Garcia and Dhont, 2005), with the HFF probably being the fault with the highest plate movement (Homberg et al., 2010). Normal and strike-slip motion in the TFZ cause the high seismic activity (Gudmundsson et al., 1993; Rögnvaldsson et al., 1998). Numerical modelling shows that the stress field geometry within the transform zone is complex and includes stress deflections close to, but also away from the major faults (Homberg et al., 2010).

Out of the three lineaments, only the HFF has a clear onshore expression (Gudmundsson et al., 1993; Mariotto et al., 2014; Garcia and Dhont, 2005). The HFF is marked by land surface depressions occupied by lakes and fault scarps which sometimes exceed 200 m in height, indicating a significant normal component (Gudmundsson et al., 1993). The right-lateral displacement is at least 5 – 10 km (Gudmundsson et al., 1993). A possible buried continuation of the HFF towards the SE has been suggested on the basis of fracture distribution within the Krafla fissure swarm as well as earthquake epicentres in this area (Hjartardóttir et al., 2012). The DAL can be traced seismically (Garcia and Dhont, 2005; Rögnvaldsson et al., 1998) with earthquakes up to M 6.2 in 1934 near Dalvík city (Rögnvaldsson et al., 1998). The onshore part of the fault shows little or no structural evidence (Rögnvaldsson et al., 1998). As for the DAL, the GRL shows no onshore structural evidence but can be traced offshore based on seismicity (Garcia and Dhont, 2005; Rögnvaldsson et al., 1998). The fault seems to have an “en échelon” structure rather than being continuous (Rögnvaldsson et al., 1998).

2.2. Earthquakes

From the start of the well monitoring at HU-01 and HA-01, three earthquakes of M > 5 have occurred in the study area, each of which has coincided with hydrochemical changes: 16 September 2002 (M 5.8) (66.938°N 18.456°W), 21 October 2012 (M 5.6) (66.309°N 18.666°W), and 2 April 2013 (M 5.3) (66.426°N 17.599°W) (Skelton et al., 2019, 2014) (Fig. 1 b). The epicenters of the 16 September 2002 and 2 April 2013 earthquakes were located within the GRL and were caused by right-lateral strike slip fault motion, and the epicenter of the 21 October 2012 earthquake was located close to the intersection of the HFF and KR and caused by normal fault motion (Skelton et al., 2019). The 16 September 2002 earthquake caused dilatational strain of the order 2.8×10^{-9} at HU-01 and dilatational strain of the order 1.9×10^{-9} at HA-01; the 21 October 2012 earthquake caused dilatational strain of the order 2.8×10^{-10} at HU-01 and compressional strain of the order 1.1×10^{-9} at HA-01; and the 2 April 2013 earthquake caused dilatational strain of the order 4.1×10^{-9} at HU-01 and dilatational strain of the order 1.6×10^{-9} at HA-01 (Skelton et al., 2019).

2.3. Geology

The study area is a 1.5 km wide N – S trending valley characterized by glacial erosion (Fig. 1c). Topographically, the mountains bordering the valley reach elevations of approximately 1 000 m.a.s.l. in the west and 700 m.a.s.l. in the east. Elongated N - S trending hills are located on the valley floor and reach elevations of 200 m.a.s.l.. The mountain Bárðarbunga under the Vatnajökull glacier, which is part of the river recharge area, reaches an elevation of 2 000 m.a.s.l. and is located approximately 150 km south of the sampling area.

The bedrock in the study area mainly consists of mafic and intermediate lavas from Tertiary to Holocene ages with intercalated sediments (Jóhannesson, 2014) (Fig. 2). The valley floor is covered with the youngest lavas of Postglacial age (Jóhannesson, 2014). The sandur in the northern part of the valley comprises Holocene sediments (Jóhannesson, 2014). There is a general dip (< 10 °) of the lava beds to the E or SE in the study area (Jóhannesson and Sæmundsson, 2009). Geological rift structures, such as faults, dykes and sub-glacially formed ridges of pillow lavas and tuffs do not show clear expressions in the study area, but do so further east in the NVZ, where they generally strike in a N - S direction (Jóhannesson and Sæmundsson, 2009).

Subsurface lithology is revealed from core log documentations from borehole drillings. Boreholes with available documentation in the study area include HA-04 (N65°52.332', W017°27.165'), HA-01, AA-01 (N65°52.504', W017°24.325') and HU-01. Geological profiles of the boreholes HA-04 and AA-01 are shown in Figure 2.

The 123 m deep borehole HA-04, which was drilled in 1996, is cased down to 51 m, located 20 m from HA-01 and penetrates from bottom to top: basalt layers of varying grain size and lava clinker from 123 – 57 m, sandstone from 57 – 54 m, basalt layers of varying grain size and lava clinker from 54 – 35 m, sandstone from 35 – 30 m, clayey, sandy sediment from 30 – 21 m, and basalt

from 21 -0 m (Friðleifsson, 1997). The well is flowing artesian. The water inlets are at 104 m, 78 – 81 m, and 60 m, and it is likely that the water runs between layers (Friðleifsson, 1997).

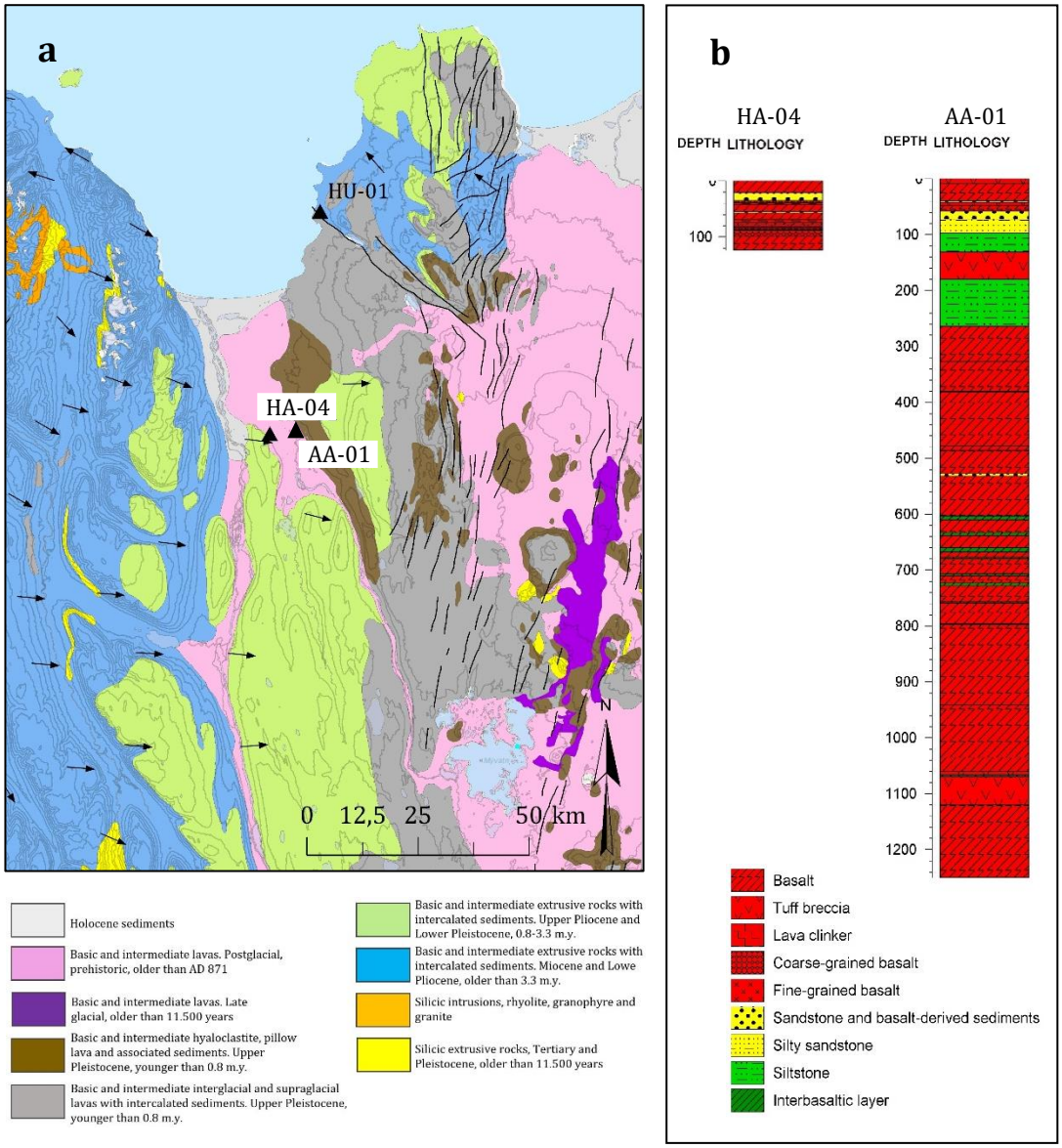

Figure 2. a) Geological map of the study area (Jóhannesson, 2014), and the locations of the HU-01, HA-04 and AA-01 boreholes. The arrows show dip direction (dip < 10˚) and the lines show fractures of the NVZ (Jóhannesson and Sæmundsson, 2009). **b)** Geological profiles of the boreholes HA-04 and AA-01 showing the core logs. The core log from HA-04 is reworked from Friðleifsson (1997) and AA-01 is reworked from Sæmundsson et al. (1976).

The 101 m deep borehole HA-01, which was drilled in 1964, is cased down to 35 m, and penetrates from bottom to top: basalt from 101 – 42 m, basalt derived sediments and sand/sandstone from 42 – 21 m, and basalt from 21 – 0 m, according to an unpublished drill report by Rafmagnveitur Ríksins Jarðborunardeild (1964) summarized by Andrén et al. (2016). The well is flowing artesian with an approximate discharge of 7.7 l/s (Skelton et al.,

2019). The water inlets are at 97.5 m, 81.5 m, and 65 m, as summarized by Andrén et al. (2016).

The 1 250 m deep Árnes borehole, AA-01, which was drilled in 1975, is cased down to 294 m, located 5 km east of HA-01 and HA-04, and penetrates from bottom to top: a sequence of interlayered basalt and interbasaltic layers (which are often composed of clayey organic-rich material (Einarsson, 1994)) from 1 250 – 265 m including a 60 m thick tuff layer encountered at around 1 100 m, siltstone from 265 – 180 m, tuff from 180 – 130 m, siltstone from 130 – 97 m, sandstone from 97 – 59 m, basalt from 59 – 48 m, tuff from 48 – 42 m, sandstone from 42 – 39 m including a palaeosol at 39 m depth, basalt from 39 – 8 m and tuff from 8 – 0 m. (Sæmundsson et al., 1976). Aquifers are encountered at ca. 1 110 - 1 130 m (small aquifers), 810 – 825 m, and 260 m (Sæmundsson et al., 1976). The well is flowing artesian and the discharge is a few l/min (Björnsson and Hjartason, 2001).

The 1 506 m deep borehole HU-01, which was drilled in 1961, is cased down to 173 m, located on the Tjörnes peninsula and penetrates from bottom to top: interlayered basalt and sandstone from 1 506 - 1 400 m, clayey conglomerate from 1 400 - 1 387 m, basalt including two thin sandstone layers from 1 387 - 1 151 m, sandy claystone from 1 151 - 1 070 m, clayey conglomerate from 1 070 - 1 030 m, a thick sequence of interlayered sandstone, claystone, clayey conglomerate, basalt, zeolite facies altered rock (partly brecciated), and clayey breccia from 1 030 – 742 m, and partly brecciated sandy and clayey tillite from 742 – 0 m (Tómasson et al., 1969). The HU-01 borehole is nonflowing artesian and the water rises to ~ 20 m below the surface from where it is pumped to the surface at a rate of 0.5 l/s (Skelton et al., 2019). The water inlets are at 1 388 m (5 l/s), 1 220 m (0,8 l/s), 730 m, 702 m, 488 m (0,7 l/s) (Tómasson et al., 1969). The geological sequence of the Tjörnes peninsula is vertically and laterally displaced by the HFF (Einarsson, 1994; Tómasson et al., 1969). The borehole HU-01 is located on the HFF (Tómasson et al., 1969; Wästeby et al., 2014), and might cross the fault zone close to 1 200 m (Wästeby et al., 2014).

The geothermal gradient is about 90 ˚C/km at HU-01 based on zeolite facies altered rocks uplifted at the coast at Heiðinshöfdi and the in situ temperature of the water at 1 000 - 1 200 m depth at HU-01 (94 ˚C) (Wästeby et al., 2014). The geothermal gradient at AA-01 is similar, based on water temperatures from the drill report (Sæmundsson et al., 1976). The water temperature at AA-01 is 11 ˚C at 0 m, 74 ˚C at 800 m and 97 ˚C at 1 160 m (Sæmundsson et al., 1976).

The general features of subsurface geology common to the boreholes is a base sequence of, probably shallowly dipping, layered tertiary basalt with interbasaltic layers. The tertiary basalt is overlain by a, probably shallowly dipping to horizontally layered, sedimentary sequence of varying composition with intercalated lava flows. Brecciated rocks in the boreholes indicate faulting in the bedrock. Artesian flow in boreholes indicate the presence of confined aquifer(s). Observations made during borehole drillings indicate that

groundwater flows between layers (Friðleifsson, 1997; Sæmundsson et al., 1976).

2.4. Hydrology

The annual precipitation in the study area varies from 500 mm in the sampling area to 4 000 mm in the Skjálfandafljót recharge area at the glacier Vatnajökull in the south (Einarsson, 1994). The glacial-fed river Skjálfandafljót and the lake-fed river Laxá, originating from lake Mývatn, flow northwards through the study area and drain into the sea in the bay Skjálfandi (Fig. 3). The mean annual temperature in the study area is 3.2 ˚C, and the mean temperatures in January and July are - 2.2 ˚C and 10.5 ˚C, respectively (Einarsson, 1994).

The ice sheet of the last glaciation retreated from the coast about 11 000 years ago in the area, and about 10 000 years ago it was reduced to its approximate present-day extent (Andrés et al., 2019). The sea probably flooded the lowland up to about 30 – 60 m above present-day sea level after deglaciation, which is the highest sea level in many parts of Iceland since the last glaciation (Einarsson, 1994). Eustatic rebound of about 5 m per century then caused a regression and a shoreline that lay further out than at the present day between 9 000 and 3 000 years ago. From 3 000 years ago and until the present day the shoreline has probably had its present location (Einarsson, 1994). In earlier times, from the Tertiary and until the Holocene, lavas intercalate with marine sediments, lignite, glacial tills, sandstones and siltstones, expressed in a sedimentary sequence on the Tjörnes peninsula, indicating a variable climate as well as variations in sea level with repeated transgressions and regressions (Einarsson, 1994).

The sampling area is located in a geothermal low-temperature area (Arnórsson, 1995). Geothermal areas are traditionally divided into low temperature areas (water temperature ~ 100 ˚C at 1 000 m depth) and high temperature areas (water temperature ≥ 150 ˚C at 1 000 m depth) (Bodvarsson, 1961). They are commonly associated with permeable rock formations and active tectonics (Arnórsson, 1995). Waters in low-temperature systems are typically alkaline, and temperature is the main variable controlling water composition, including pH (Arnórsson et al., 1983).

Permeability in Icelandic basalt is largely controlled by the degree of hydrothermal alteration, involving formation of secondary minerals in vesicles and fractures, with the degree of alteration increasing with depth (Walker, 1960). Tertiary basalts in Iceland are generally the most impermeable, since they have formed first and have mostly been buried deeper, whereas post-glacial basalts are the most permeable, with a difference of 6 – 7 orders of magnitude between the two (Saemundsson and Frithleifsson, 1980). Seismic data indicate that the pores of the basalt are almost completely filled with secondary minerals at an approximate depth of 3 km (Flovenz et al., 1985), and the maximum depth of groundwater convection in low-temperature areas is probably 2 – 4 km for that reason (Arnórsson, 1995). Non-isotropic permeability, caused by intercalation of permeable and impermeable beds, for example where clay and Tertiary basalt and sediments alternate, or caused by

faults, dykes and fractures, also influence groundwater flow (Einarsson, 1994). Such non-isotropic permeability often causes springs to occur in spring lines downslope of mountains, since they are often controlled by the bedding dip of low permeable beds, as well as thermal springs to emerge by fault and dykes in low-temperature areas (Einarsson, 1994).

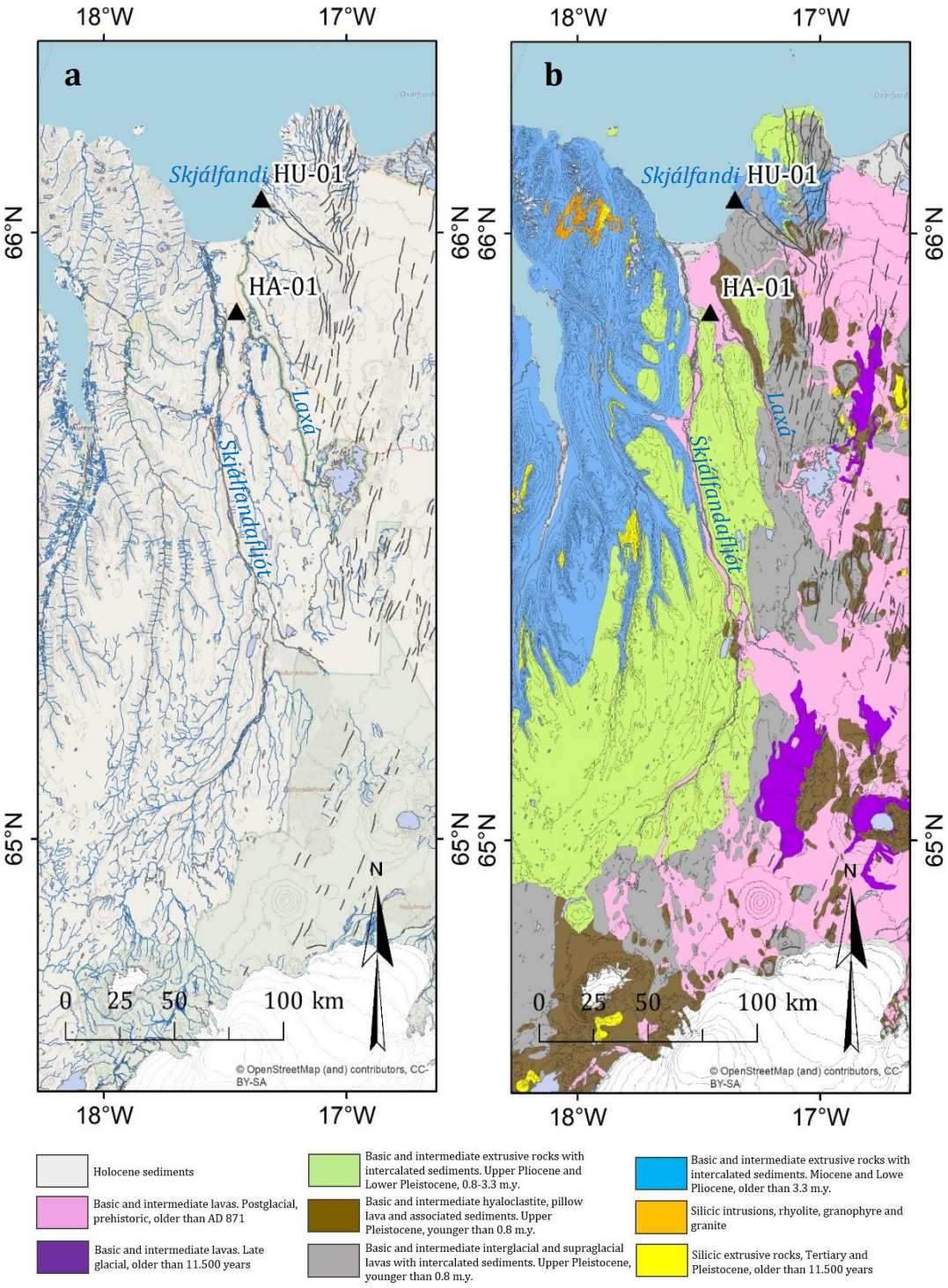

Figure 3. a) River tributaries, recharge area and drainage patterns for the rivers Skjálfandafljót and Laxá. **b)** Geological map for the area underlying the Skjálfandafljót and Laxá watershed (Jóhannesson, 2014).

Most surface waters and cold groundwaters on Iceland show Cl concentrations corresponding to those of local precipitation, but some low-temperature geothermal waters in lowland areas show elevated Cl concentrations due to direct seawater infiltration into the bedrock (Arnórsson et al., 1983), or due to leaching of marine sediments formed during a time when the lowlands were submerged below sea level (Arnórsson, 1995).

The Cl content at HU-01, located at the coast, is high (1 700 ± 20 ppm), and indicates mixing with an 8 – 10 % seawater component at this site (Wästeby et al., 2014). Also, the Cl content at Húsavik seems to increase with depth but is low at Hafralækur, further inland (Árnason, 1976).

Deuterium (^2H) is a stable hydrogen isotope. Since deuterium is almost twice as heavy as hydrogen (^1H), very little ^2H evaporates from the ocean into water vapor (H_2O) and is contained in clouds. With lower temperatures, even less deuterium evaporates and the fraction of deuterium (δ^2H) in precipitation becomes very low. The deuterium content in precipitation is further controlled by distance from the coast, altitude and latitude, with δ^2H values becoming lower with increasing distance from the coast, higher altitude and higher latitude (Árnason, 1977). This is an effect of a quicker rainout of water molecules containing the heavier isotope when the water vapor cools down. The same behaviour is true for the stable oxygen isotope ^{18}O, which is heavier than the more common stable oxygen isotope ^{16}O.

When measuring the δ^2H content in groundwater, the δ^2H value of a water sample from e.g. a spring or a stream gives the average δ^2H value of the precipitation in the catchment area belonging to that sample point (Árnason, 1977). Based on deuterium measurements of waters from springs, rivers, wells and winter snow accumulation on glaciers, Árnason (1977, 1976) constructed a deuterium map over Iceland which shows the present-day distribution of δ^2H in precipitation throughout the country, as well as the recharge areas and general flow paths of the geothermal groundwater (Fig. 4). In Iceland, the lowest δ^2H values are found at Vatnajökull (- 106 ‰) and the highest are found at the southwest coast (- 50 ‰) (Árnason, 1977, 1976). The δ^2H values in the sampling area range from approximately – 95 ‰ inland to – 70 ‰ at the coast (Árnason, 1977, 1976).

The Husavik-Hafralækur area shows a complex distribution of waters originating from precipitation at different latitudes and altitudes and of different ages, and a mixing of these waters (Árnason, 1976). The oxygen and hydrogen isotopes of these waters follow the global meteoric water line (GMWL) (Craig, 1961), indicating a meteoric origin of the waters (Árnason, 1976).

Low measured deuterium content of waters at Húsavik and Hafralækur is proposed to originate from precipitation from the interior of Iceland during a much colder climate regime than today, > 10 000 years ago, since they are lower than in any precipitation on Iceland today (Árnason, 1977, 1976). The hot springs and wells at Húsavik, Hafralækur, Reykjahverfi, Laugar and Marteinsflæða are proposed to be derived from a main thermal groundwater stream flowing from the glacier Vatnajökull to the north coast (Árnason,

1976). According to this model, there is an age gradient from the coast to the interior in the geothermal waters, with the oldest waters located at the coast.

Another possible model is that old waters, often localized to Icelandic lowlands and flat ground close to sea level, originates from glacial meltwater when the glaciers retreated ~ 10 000 - 15 000 years ago, that percolated into the ground and became stagnant hydrologically (Stefánsson et al., 2017). According to this model, there is no age gradient in the geothermal waters towards the coast.

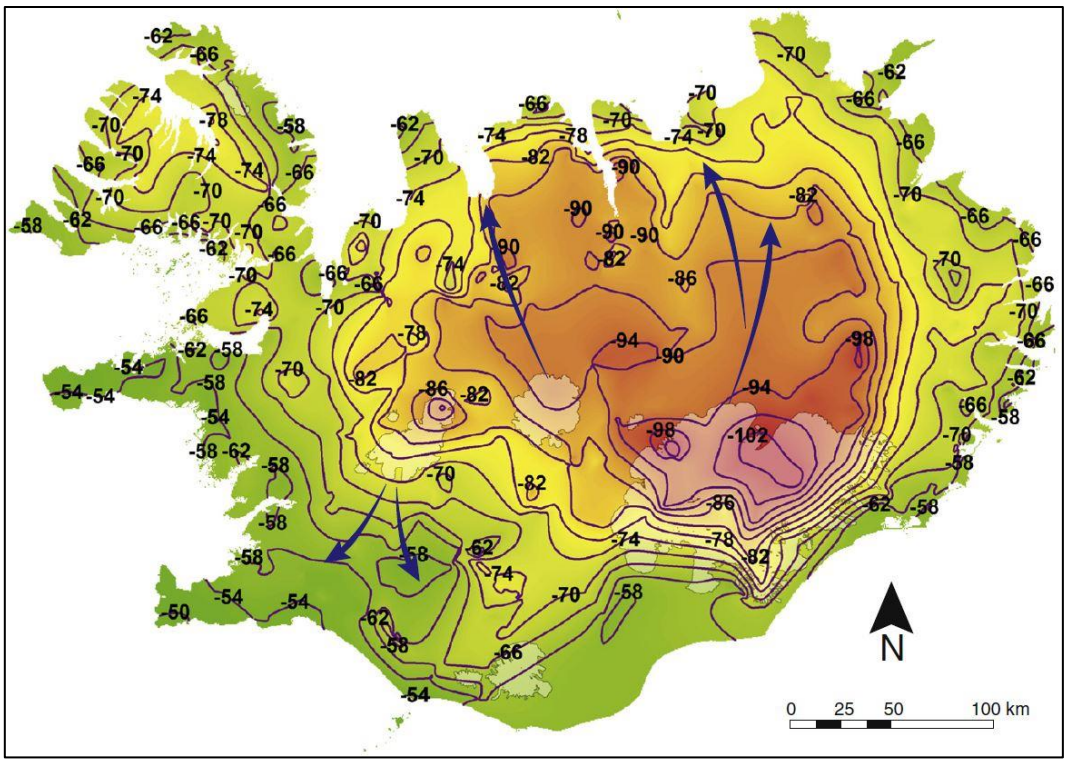

Figure 4. Map showing the δ^2H distribution in precipitation on Iceland and the possible recharge areas of general groundwater flow feeding the geothermal systems. The map is based on Árnason (1977, 1976) and is reworked and published by Stefánsson et al. (2017).

2.5. Hypotheses

The aim of this project is to map the different aquifers in the Húsavik-Hafralækur area, trace the sources and flow paths of these waters and construct a conceptual hydrological model of the area. This will be done by analyzing the chemistry of groundwater samples from different aquifers. The results will be used to test three proposed hypotheses about the hydrogeology in the area: (1) There is a seawater gradient from the coast to the interior. (2) There is an age gradient of the groundwater from the coast to the interior. (3) A source of the groundwater is ice caps.

3. Methods

3.1. Tracers used for water sources and mixing

The use of stable isotopes (δ^2H and $\delta^{18}O$) is a common method to trace water sources and has been widely used in hydrogeological studies on Iceland since the pioneering works by Craig (1961) and Friedman et al. (1963), but no detailed study has yet been conducted in the Húsavik - Hafralækur area. Conservative elements, such as Cl and B, are useful tracers for meteoric water and seawater sources, and a mixing of those sources with rock (Arnórsson and Andrésdóttir, 1995).

While the water is sampled and analysed for a suite of parameters (pH, SiO_2, Na, K, Mg, Fe, Al, B, SO_4, Cl, F, Mn, Br, Mo, Sr, Ti, P, Li, CO_2, δ^2H, δ^3H, $\delta^{18}O$ and Temperature), this study focuses on the stable isotopes (δ^2H and $\delta^{18}O$) as well as the elements Cl and B, due to their near to conservative behaviour in Icelandic low-temperature geothermal waters (Arnórsson and Andrésdóttir, 1995). Covariations of other parameters with Cl, B, δ^3H, and $\delta^{18}O$ are used to investigate coupling with hydrogeochemical changes at HU-01 and HA-01. Visualization of the measured concentrations and values on geographical maps are also used to reveal major distribution patterns and help trace water sources, flow paths and water-rock interaction.

3.2. Sampling and analysis

Water samples were collected in June 2018 from 13 springs, 10 rivers, 10 streams, 2 lakes and 6 boreholes at 41 sampling sites.

Depending on the conditions at the sampling site, the sampling bottles were either directly submerged and filled up under water (in the case of unfiltered samples), a jug was used to scoop out water and fill up the bottles, or a funnel with a silicone tube was used to collect the water if the discharge was low. All bottles and sampling equipment were carefully rinsed three times with the sampling water before use. All glass bottles were filled completely so that no air bubbles remained.

3.3. Elemental analysis

All samples for analysis of the elements Si, Na, K, Mg, Fe, Al, B, Mn, Mo, Br, Sr, Ti, P, Li SO_4, F, and Cl were filtered through a 0,2 µm cellulose acetate filter (Advantec® C020A047A) using a hand-held filtration unit consisting of a vacuum pump (Mityvac®) combined with a vacuum container (Nalgene®; max pressure 1 Bar) and collected into 40 ml poly propylene bottles.

Samples collected for analysis of the elements Si, Na, K, Mg, Fe, Al, B, Mn, Mo, Br, Sr, Ti, P and Li were then acidified with 0,4 ml suprapure concentrated HNO_3 per 40 ml water using a pipette (Finnpipette® 100 – 1000 µl). The elemental analysis was conducted at the University of Iceland by inductively coupled plasma optical emission spectrometry (ICP-OES) in October 2018. Samples collected for analysis of the elements SO_4, F, and Cl were not further

treated, and elemental analysis was conducted at the University of Iceland by ion chromatography (IC) in October 2018.

3.4. Water temperature, pH and CO_2

Water temperature was measured in the field using a portable thermometer (Digi-Sense.® 20250-18). Samples collected for analysis of pH (60 ml) and CO_2 (250 ml) were collected into amber glass bottles. The water was not filtered or acidified. pH and CO_2 were analysed at room temperature (~ 20 ˚C) within 48 hours. pH was measured using a portable pH meter (Metrohm® 826 pH mobile) with an integrated electrode and CO_2 was measured through titration.

The pH meter was calibrated at room temperature before measurements of the water samples, using two buffers of pH 4 and 7. The electrode was rinsed with plenty of deionized (DI) water between each measurement and the excess water was wiped off without touching the membrane. During the measurements, the water was stirred with a magnetic stirrer (DP Cole-Parmer®) and a magnetic stirring bar in a 100 ml glass breaker.

Total dissolved inorganic carbonate (CO_2) was determined through acid-based titration from pH 8.3 to pH 4.5 using 0,1 M HCl and a portable pH meter, a 100 ml glass breaker, a magnetic stirrer and a stirring bar as for the pH measurements described above. A volumetric flask (50 ml) was used to measure 50 ml of the sample water into the glass breaker. The electrode was placed into the sample water and the pH was adjusted to 8.3 by adding acid (0.1 M HCl) or base (0.1 M NaOH) as needed using two separate 2 ml microburettes. The sample was then titrated from pH 8.3 to pH 4.5 using a 0.1 M HCl solution in a 2 ml microburette. The millilitre amount of titrant (HCl) was recorded and the CO_2 concentration was calculated by using:

$$CO_2(ppm) = \frac{ml\ HCl * Molarity\ HCl}{ml\ sample} * 44000$$

3.5. Stable isotopes

Samples for δ^2H and $\delta^{18}O$ (60 ml) analysis were collected in amber glass bottles. The water was not filtered or acidified. Oxygen and hydrogen isotopes were analysed using a Finnegan MAT 251 ion ratio mass spectrometer (IRMS) at the University of Iceland and the results were reported as conventional δ-values in ‰ relative to the VSMOW standard.

3.6. Distribution maps

The isotope and elemental distribution maps were generated with ArcGIS using inverse distance weighted (IDW) interpolation for the measured values with the settings: Power: 2; Neighbourhood type: Standard; Maximum neighbours: 3; Minimum neighbours: 2; Sector type: 4 Sectors; Angle: 0.

4. Results

The chemical and isotopic compositions were determined for cold waters from springs, rivers, streams, lakes and boreholes and for low-temperature geothermal waters from springs and boreholes in the Húsavik-Hafralækur area. The sample locations are shown in Figure 6 and the results are listed in Table 1. Water temperatures range from 2.8 ˚C to 97.5 ˚C (n = 41) and pH range from 7.14 to 10.58 (n = 41). Boron concentrations range from 0.012 to 0.125 ppm (n = 18) with 23 samples having concentrations under the detection limit (< 0.01 ppm). Chlorine concentrations range from 1.6 to 1 710 ppm (n = 41). The $\delta^{18}O$ values range from -17.0 to -8.1 ‰ (n = 41), and the $\delta^{2}H$ values range from - 128 to - 58.5 ‰ (n = 41). The altitudes for the sample locations range from 3 to 277 m.a.s.l. (n = 41). Concentrations of CO_2, SiO_4, Na, K, Ca, Mg, Fe, Al, SO4, Sr, Mn, Br, Mo, Ti, P, Li, and F are presented in Appendix A.

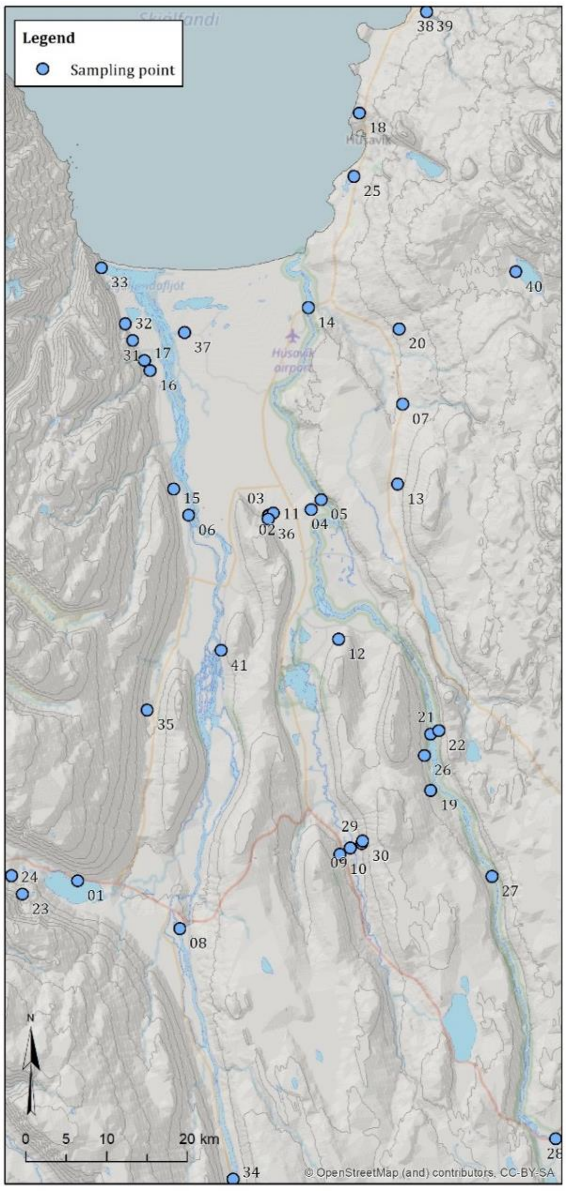

Figure 6. The study area and the sampling locations. The dots show the sampling locations and the sampling numbers.

Table 1. Chlorine and B concentrations, δ^2H and $\delta^{18}O$ values, Temperature, altitude, and pH of the sampled waters in the Húsavik-Hafralækur area.

No.	Location	Type	Temp (°C)	pH	B (ppm)	Cl (ppm)	$\delta^{18}O$ (‰)	δ^2H (‰)	Altitude (m.a.s.l.)
1	Ljósavatn	Lake	10	7,4	< 0.01	4,0	-11,5	-80	117
2	Hafralækur HA-01	Borehole	70	10,2	0,050	9,9	-16,8	-126	26
3	Hafralækur HA-04	Borehole	61	10,2	0,051	9,8	-16,8	-126	26
4	Árnes AA-01	Borehole	8	10,2	0,053	8,5	-17,0	-128	32
5	Laxá by Árnes	River	12	8,6	0,022	3,7	-11,7	-86	31
6	Skjálfandafljót by Geirbjarnarstaðir	River	12	7,7	< 0.01	3,7	-11,8	-83	11
7	Þverá by Road 87	Stream	13	7,8	< 0.01	8,1	-10,9	-75	106
8	Skjálfandafljót by Goðafoss	River	13	7,9	< 0.01	1,6	-12,8	-92	125
9	Reykjadalsá by Laugar	Stream	14	8,1	< 0.01	4,9	-10,6	-77	47
10	Laugar by Lautavegur	Spring	5	7,5	< 0.01	6,8	-11,3	-78	98
11	Hafralækur stream by bridge	Stream	8	8,0	< 0.01	6,9	-10,9	-78	31
12	Múlatorfa by Múli II	Spring	5	7,9	< 0.01	10,4	-11,0	-75	112
13	Hveravellir by geyser	Spring	86	9,5	0,066	11,9	-13,1	-97	148
14	Laxá by bridge	River	13	8,6	0,025	3,9	-11,8	-86	9
15	South of Geirbjarnarstaðir	Stream	5	7,4	< 0.01	9,6	-10,5	-73	48
16	Nípá River by Nípá farm	River	5	7,1	< 0.01	4,1	-11,0	-74	11
17	North of Núpá	Spring	11	7,8	< 0.01	9,5	-9,8	-66	9
18	Húsavík HU-01	Borehole	98	9,0	0,125	1709,5	-15,0	-122	69
19	Halldórsstaðir	Stream	11	8,1	< 0.01	7,5	-10,5	-75	179
20	Above Skarðaborg	Spring	4	8,7	< 0.01	10,3	-11,1	-75	138
21	Laxá by Sogsbrú	River	14	9,3	0,022	3,7	-11,9	-85	132
22	Hills east of Sogsbrú	Spring	11	9,3	< 0.01	7,8	-11,5	-80	173
23	Stóridalur by Stórutjarnir	Spring	7	7,6	< 0.01	2,8	-12,1	-85	268
24	Stórutjarnir ST-04	Borehole	66	9,7	0,114	16,2	-13,8	-101	177
25	Haukamýri	Spring	3	8,7	< 0.01	11,3	-10,7	-72	33
26	North of Halldórsstaðir	Spring	7	7,6	< 0.01	8,0	-11,2	-77	163
27	Laxá by Ferjuhöfn	River	11	8,3	0,025	3,4	-12,0	-87	151
28	Laxá exiting Mývatn	River	12	9,0	0,029	3,3	-11,9	-87	269
29	East of Laugar	Spring	46	10,6	0,062	7,2	-14,5	-104	120
30	East of Laugar	Spring	5	7,5	< 0.01	6,8	-11,1	-77	137
31	West of Björg farm	Spring	5	7,3	< 0.01	9,1	-9,9	-70	57
32	North of Björg	Stream	9	7,4	< 0.01	8,2	-10,3	-69	8
33	North of Bjargakrókur	Stream	8	7,7	< 0.01	9,3	-9,5	-67	3
34	Skjálfandafljót by Sandhaugur	River	10	7,7	< 0.01	1,6	-12,6	-90	185
35	Gljúfurá by Hlíð farm	Stream	10	7,5	< 0.01	4,0	-11,6	-81	71
36	West of Hafralækur	Stream	9	7,8	0,013	10,5	-10,5	-73	39
37	Berg BE-01	Borehole	7	8,4	0,030	8,0	-12,2	-88	7
38	Kaldakvísl	Stream	16	8,0	0,015	9,2	-10,2	-69	41
39	South of Kaldakvísl	Spring	10	7,7	0,022	15,1	-9,6	-67	46
40	Höskuldsvatn	Lake	17	7,3	0,012	7,3	-8,1	-58	277
41	Skjálfandafljót	River	13	8,0	0,016	2,1	-12,7	-91	16

5. Discussion

The following discussion will be organized around the stated hypotheses: (1) There is a seawater gradient from the coast to the interior. (2) There is an age gradient of the groundwater from the coast to the interior. (3) A source of the groundwater is ice caps. The discussion will include a short section about the distribution of the major elements in the area. The interpretations will be summarized and visualized in a conceptual hydrogeological model based on which the hypotheses will be tested. Finally, the implications of the study will be discussed.

5.1. Seawater gradient

Some lowland areas in Iceland show elevated Cl concentrations due to seawater infiltration into the bedrock (Arnórsson et al., 1983), or due to leaching of marine sediments contained in the rock sequence (Arnórsson, 1995). Chlorine (and B) in groundwater can also originate from basalt leaching, seawater spray and aerosols in precipitation, and magma intrusions (in high-temperature areas) (Arnórsson and Andrésdóttir, 1995).

The results show that most cold and hot waters in the Húsavik-Hafralækur area contain between 1.6 ppm and 16 ppm Cl with the lowest concentrations inland and the highest concentrations at the coast (Fig. 7). This corresponds to Cl concentrations of local precipitation, which can be as low as 1 ppm inland and increase to 10 – 20 ppm at the coast (Arnórsson and Andrésdóttir, 1995), indicating a mainly atmospheric source for Cl in the area. This subtle Cl gradient may be an effect of Cl contained in seawater spray and aerosols carried by winds from the sea (Orme et al., 2015).

Very high Cl values are found at one site; the HU-01 borehole located at the coast, with a Cl content of 1 710 ppm. Such a high Cl value cannot be explained by water-rock interaction, since the Cl content of basalt is too low (90 – 190 ppm) (Arnórsson, 1995; Arnórsson and Andrésdóttir, 1995). Leaching of marine sediments is also unlikely to have caused the high Cl values, since this would affect other boreholes in the area too, which is not the case. A more likely explanation is that the HU-01 borehole is affected by seawater intrusion as has been proposed by Árnason (1976) and Wästeby et al. (2014). The calculated seawater component at HU-01 would be around 9.4 %, based on the Cl measurement of this study (1 710 ppm), the Cl concentration of seawater (19 000 ppm) (Arnórsson and Andrésdóttir, 1995), and a meteoric Cl concentration of 10 ppm. This agrees well with the estimate of Wästeby et al. (2014).

The evidence that seawater infiltrates into the bedrock at the coast, means that there is a seawater gradient in the area. However, it is not clear what this seawater gradient looks like and how far inland it extends. Since it does not seem to affect other boreholes further inland, any gradient if present must be steep and localised to coastal areas. Because Árnason (1976) measured an increase in Cl concentration with depth in wells in Húsavik, and the main

aquifer at HU-01 is proposed to be located below 1200 m (Claesson et al., 2007, 2004; Tómasson et al., 1969; Wästeby et al., 2014), it is possible that this seawater intrusion occurred only at depth. A speculation is that seawater intrusion may occur through structures of secondary permeability, since the borehole is located on the active HFF.

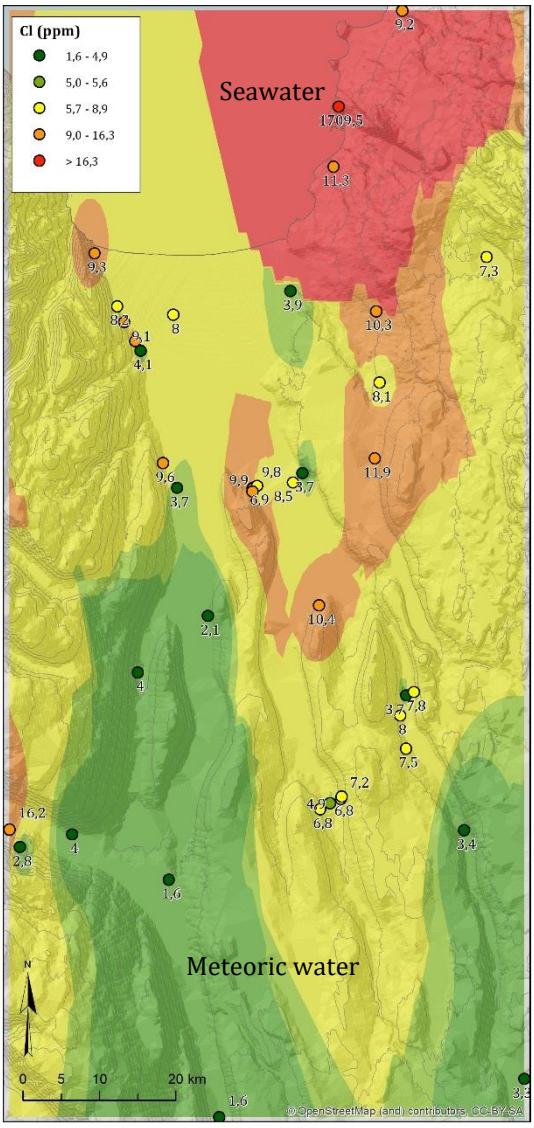

Figure 7. Map showing the distribution of Cl contents (ppm). The sample points and the measured values are shown on the map. The general Cl gradient visible in the map is an effect of rainout, but the high Cl value at the coast shows the seawater gradient.

5.2. Age gradient

Groundwater age is normally defined as the average time elapsed since the water precipitated from atmosphere. In the Húsavik-Hafralækur area, waters of both modern and pre-Holocene age have been observed, and it has been

proposed that the distribution of these waters displays an age gradient from the coast to the interior based on δ^2H measurements (Árnason, 1976).

Stable isotope ratios (δ^2H and $\delta^{18}O$) in precipitation have not changed greatly for the past 8 000 years (Árnason, 1976). This implies that the δ^2H values younger than 8 000 years are comparable to present day values (Árnason, 1977, 1976) (Fig.4). Based on $\delta^{18}O$ values from ice core studies, the corresponding δ^2H values of precipitation deposited 10 000 - 60 000 years ago were probably 50 ‰ to 100 ‰ lower than today (Árnason, 1977, 1976). Consequently, if the age of the groundwater is somewhere between 10 000 and 60 000 years, this would be expressed in exceptionally low δ^2H values; below the lowest precipitation concentrations on Iceland today (< - 106 ‰).

The waters in the Húsavik-Hafralækur area plot along the global meteoric water line (GMWL) (Craig, 1961) and the Icelandic meteoric water line (IMWL) (Sveinbjörnsdóttir et al., 1995) (Fig. 8). This means that they are of meteoric origin. The slight shift to right of the GMWL and IMWL for some waters, towards less negative $\delta^{18}O$ values, indicates that some degree of water-rock interaction has taken place. This affects $\delta^{18}O$ values but does not affect δ^2H concentrations noticeably, since, compared to O, the H content of basalt is very low (rock contains > 40 % oxygen and << 1 % hydrogen). Since δ^2H can be considered to be generally unaffected by such exchange processes, it is used as a proxy for water age in this study.

The geographical distribution of δ^2H in the Húsavik-Hafralækur area is shown in Fig. 9. The sampled waters are both cold (3 ˚C to 16 ˚C) and hot (46 ˚C to 98 ˚C), and the variation of δ^2H (water age) with water temperature is shown in Fig. 10.

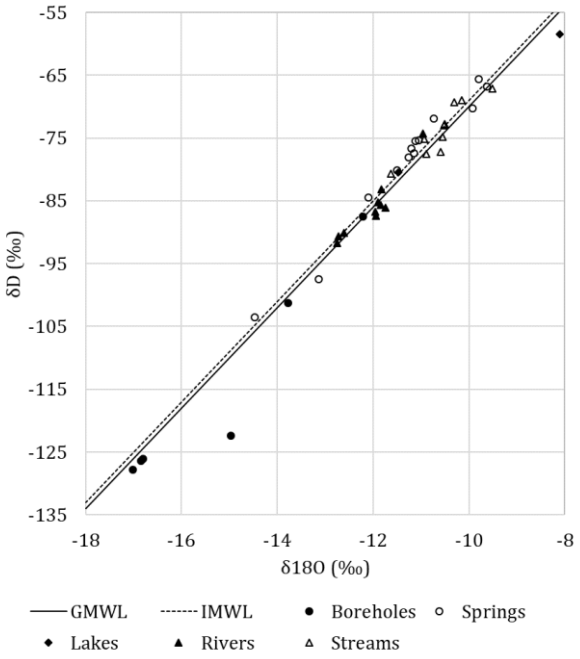

Figure 8. Bivariate plot showing the $\delta^{18}O$ and δ^2H (δD) values expressed in ‰ of Húsavik-Hafralækur waters. The waters are grouped into boreholes, springs, lakes, rivers and streams. The Global Meteoric Water Line (GMWL) (Craig, 1961) and the Icelandic Meteoric Water Line (IMWL) (Sveinbjörnsdóttir et al., 1995) are shown as well. The values plot along the GMWL and IMWL, indicating a meteoric origin of the waters. A shift to the right of the IMWL and GMWL, towards less negative $\delta^{18}O$ values indicates water-rock interaction.

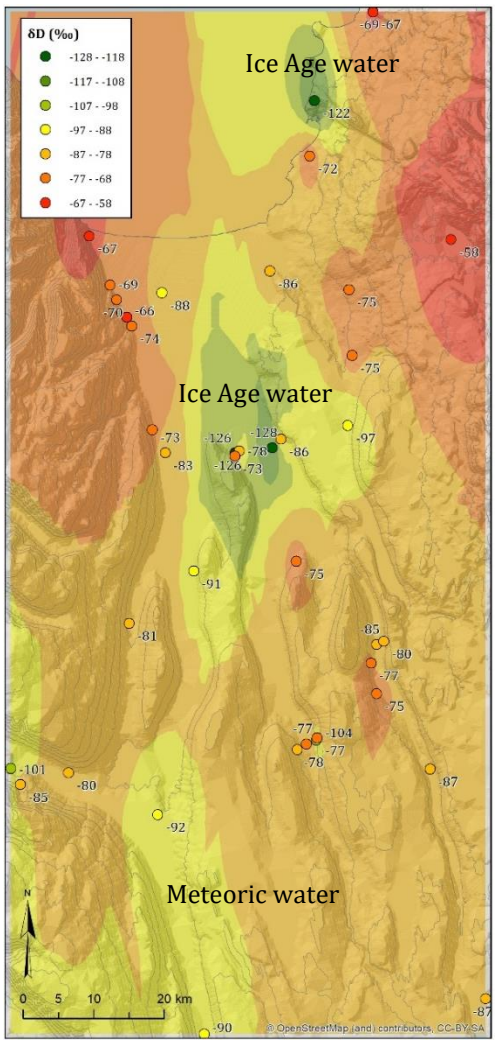

Figure 9. Map showing the distribution of δ^2H (δD) contents (‰). The sample points and the measured values are shown on the map. The figure shows that old, Ice Age waters (low δ^2H waters) are located to lowland areas close to the coast.

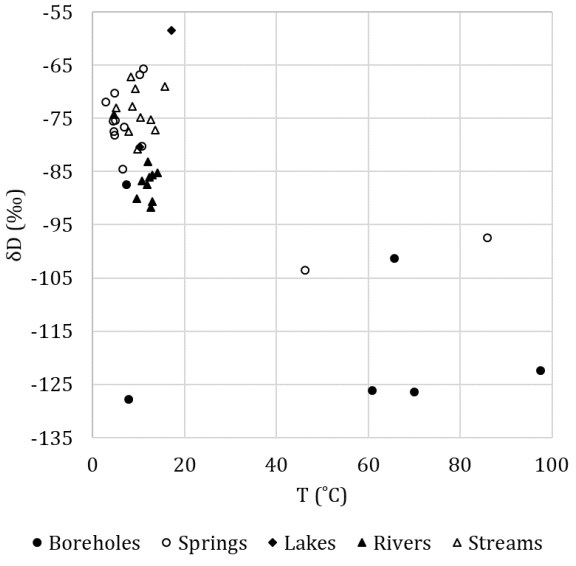

Figure 10. Bivariate plot showing δ^2H (δD) (‰) and Temperature (°C) relationship. The waters are grouped into boreholes, springs, lakes, rivers and streams. The plot shows that low δ^2H values below - 106 ‰ are found in hot waters from boreholes and δ^2H values within the present-day precipitation range (- 95 to – 70 ‰) are found in cold waters. High water temperature is interpreted to be a function of depth, due to the geothermal gradient. Thus, the figure shows that old Ice Age waters are found at depth and young waters are found at the surface.

Cold waters were collected from rivers, streams, lakes, springs and boreholes at all altitudes (3 - 277 m.a.s.l.). The cold waters show δ^2H values corresponding to those of local precipitation, indicating a modern age. They become isotopically lighter further inland, which is probably due to rainout (Árnason, 1977). The cold temperature of the waters indicates that they originate from surface waters or from shallow aquifers.

Hot waters were collected from springs and boreholes at altitudes below 177 m.a.s.l.. Some hot waters show δ^2H values that do not correspond to local precipitation but are in the range of modern precipitation deposited on glaciers in the central part of Iceland. These aquifers can either have their recharge areas at Vatnajökull and/or be a mixture of Ice Age water and modern water. Other hot waters show extremely low δ^2H values, below those of any precipitation on Iceland today, indicating that they are older than 10 000 years (Ice Age waters). Common to these waters is that they are only found in boreholes at low altitudes near sea level and close to the coast (below 69 m.a.s.l.). The high temperature of the waters indicates that they originate from deep aquifers, due to the geothermal gradient.

An exception is that the 1 250 m deep borehole at Árnes (AA-01) discharges cold Ice Age water. This indicates that the Ice Age aquifer is shallow at this location and that the 294 m deep borehole casing might be broken. According to the well owners (personal communication), the well discharged hot water for the house heating at the beginning, but after some time the water turned cold and could no longer be used for heating purposes, supporting this hypothesis.

Two models have been proposed to explain the distributions, ages, and sources of the Ice Age waters: (1) The waters originate from an ice cap at Vatnajökull and the old age is a function of the long water transport to the coast through low-permeable Tertiary basalt (Árnason, 1976). This implies that there is an age gradient from the coast to the inland in the geothermal waters. (2) The waters originate from an ice sheet and the water percolated into the ground when the ice sheet retreated. The water got stagnant in lowland areas due to the low hydrologic flow expected close to sea level (Stefánsson et al., 2017). This implies that there is no age gradient of geothermal waters from the coast to the inland.

To test model (1), first the assumed 9.4 % seawater component at HU-01 is removed. This lowers the initial δ^2H value to – 135 ‰. That makes the δ^2H value at HU-01 the lowest of the sampled waters. The borehole HU-01 is also located furthest away from Vatnajökull, compared to the other boreholes with very negative δ^2H values. The longer flow path of the water from Vatnajökull to HU-01 at the coast means that this water could be the oldest in the area.

Next, the transport time for the deep groundwater from Vatnajökull towards HU-01 is estimated. No exact value for the permeability of Tertiary basalt exists because of the high variability from one area to another, and, consequently, determination of the age of the groundwater as a function of the length of the flow path is highly speculative. However, using estimates for the transmissivity coefficient (T) of deep thermal water circulation in Tertiary

basalt from pumping tests in the Laugarnes geothermal area ($T = 3.5 \times 10^{-3}$ *to* 8.8×10^{-3} m²/s) (Thorsteinsson and Elíasson, 1970), the calculation of a possible age of the water at Húsavik would be as follows:

The coefficient of transmissivity is defined by:

$$T = k \times D$$

where T is the coefficient of transmissivity; k is the hydraulic conductivity; and D is the total thickness of the aquifers (which is assumed to be 2 000 m based on the deepest aquifer depth at Laugarnes). From this equation k is calculated, which is next used in Darcy´s law to estimate the flow velocity:

$$q = -k\frac{dh}{dl}$$

where q is specific discharge; k is hydraulic conductivity; and $-\frac{dh}{dl}$ is the hydraulic gradient, for which an altitude difference of 700 m and a distance of 150 km from Vatnajökull to Húsavik is assumed. The mean velocity (v_{mean}) of the water is found by dividing the specific discharge (q) with the effective porosity (n_{eff}). The effective porosity of Tertiary basalt is not known but a suggested value is 0.02 (Árnason, 1976 and references therein).

$$v_{mean} = \frac{q}{n_{eff}}$$

Using the assumed values, it would take between 5 000 and 12 000 years for the groundwater to reach Húsavik. This result is consistent with Ice Age water having reached HU-01 from Vatnajökull. It also points to a gradient of δ^2H values from the coast to the interior. However, it does not necessarily prove that there is an age gradient from the waters at Húsavik to the boreholes with less negative δ^2H values (HA-01, HA-04 and AA-01) that are closer to Vatnajökull. This can only be proven if it can be shown independently that δ^2H values of precipitation becomes increasingly negative with time during the Ice Age. Antarctic ice core records show that δ^2H values of precipitation becomes increasingly negative with time during the Ice Age termination but not during the Ice Age, a time period when they instead become increasingly positive (e.g. EPICA, 2004). A speculation is that the gradient of δ^2H values may reflect the time period from the Ice Age termination onwards, rather than the whole Ice Age.

Model (2) suggests that there is a reservoir of stagnant Ice Age water close to sea level, which implies a closed system. However, since there is an outflow of water from the wells as well as no apparent change in water level in the HU-01 borehole, the system cannot be completely closed. Thus model (2) is considered unlikely.

Common to both models is that hot Ice Age water rises from deep aquifers to the surface in lowland areas. However, the depths of the wells discharging hot water differ considerably. The wells at Hafralækur are only about 100 m deep, whereas the borehole at Húsavik is over 1 000 m deep. A possible explanation for this disparity is that the wells at Hafralækur penetrate a fault where hot water rises to the surface from deep aquifers. Looking at the local geomorphology, the hillslope next to Hafralækur might be the fault plane of a N-S striking normal fault, which supports this hypothesis.

The ascent of hot water in faults can be explained by hydrostatic pressure and/or that a heating source from below drives the ascent of hot water upwards in the fault. Such a model has, for example, been proposed to explain the ascent of high-temperature geothermal water in faults in the NVZ (Pope et al., 2016).

5.3. Water sources, mixing and water-rock interaction

Waters not only mix, but they also react with rocks upon contact with them. The degree of water-rock interaction is, of course, dependent on the availability of fresh rock surfaces to react with, but it is also enhanced by higher temperatures (Arnórsson et al., 1983).

In low-temperature areas, such as the Húsavik-Hafralækur area, Cl and B are considered to be generally incompatible (Arnórsson and Andrésdóttir, 1995), which make them good tracers of water sources and water-rock interaction. The relationship between the Cl/B ratio and Cl concentration in cold and low-temperature geothermal waters can reveal two processes: (1) water-rock interaction (stochiometric dissolution of Cl and B from the rock), and (2) seawater-freshwater mixing.

The Cl content of local precipitation is approximately 1 – 10 ppm (Arnórsson and Andrésdóttir, 1995) with a Cl/B ratio that corresponds to that of seawater (4 350) (Arnórsson, 1995). The typical Cl/B mass ratio for Icelandic basalts is 80 – 150 ppm and the average B value is 1.2 ppm (Arnórsson and Andrésdóttir, 1995). The water becomes enriched in B relative to Cl upon reaction with basalt until it reaches the Cl/B ratio of the rock.

The results show that the waters in the Húsavik-Hafralækur area are meteoric waters that have reacted with basalt to various degrees (Fig. 11).

Only one water sample displays mixing of meteoric water and seawater, and that is the HU-01 borehole at the coast. It can also be observed that the Cl/B ratio at this site is unusually high, which makes it plot above the seawater ratio. This indicates non-stochiometric fractionation of Cl and B, which can happen either through a gain of Cl or a loss of B in the water. Since B has been observed to be removed from seawater in reaction with basalt at low temperatures and incorporated into the mineral structure of secondary minerals such as clay (e.g. Ishikawa and Nakamura, 1992; Seyfried et al., 1984), it is inferred that this process could explain the elevated Cl/B ratio in the water at Húsavik. This is supported by the investigated fault healing process at HU-01, where the hydrochemical recovery caused precipitation of secondary minerals along fractures e.g., zeolites and clay (Wästeby et al., 2014).

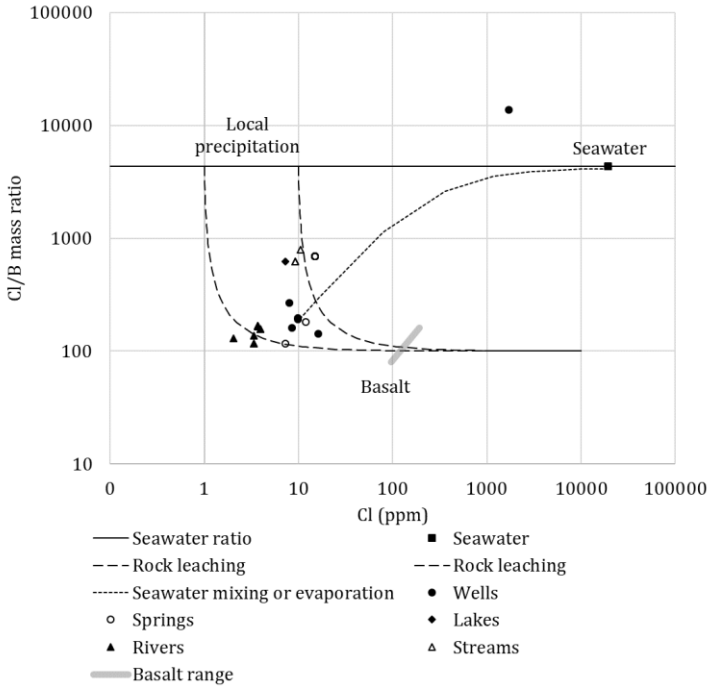

Figure 11. Relationship between Cl/B mass ratios and Cl concentrations of waters in the Húsavik-Hafralækur area. The Cl/B seawater ratio (4 350) (Arnórsson, 1995), the Cl values for local precipitation (1 - 10 ppm), the Cl values for seawater (19 000 ppm), the Cl/B mass ratio for Icelandic basalts (80 – 150) for the average B value of Icelandic basalts (1.2 ppm) (Arnórsson and Andrésdóttir, 1995) are shown as well. The two dashed rock-leaching curves represent the meteoric parent water that dissolve Cl and B from the rock in the ratio of 100 to 1 (Arnórsson, 1995). The single dashed curve represents mixture of seawater and geothermal water that has reacted with basalt. The figure shows that the waters in the Húsavik-Hafralækur area are meteoric waters that have reacted to various degrees with basalt. Mixing with seawater happens at only one site.

The relationship between the Cl/B ratio and δ^2H values reveal the relationship between the age of the waters and the degree of water-rock interaction.

It can be observed that old (low δ^2H) waters are equilibrated with Icelandic basalt (Fig. 12). This is expected, since progressive rock dissolution and the release of Cl and B from basalt in near stochiometric proportions is normal for low-temperature geothermal waters (Arnórsson and Andrésdóttir, 1995).

It can also be observed that modern age river waters are equilibrated with Icelandic basalt. The reason for this is less obvious, but Arnórsson and Andrésdóttir (1995) suggest that cold waters can receive B from basaltic rock powder from glacial erosion which is often remobilized by wind erosion in Iceland. Since the sediment load in the rivers is high, and probably consists of great amounts of fine-ground basaltic rock powder, the rock leaching could possibly be explained by reaction of the river water with this fine-grained material.

Finally, modern age cold surface waters show a very small degree of water-rock interaction. The small degree of rock leaching in these waters is best

explained by addition of B from atmospheric dust (Arnórsson and Andrésdóttir, 1995), since dissolution of air borne dust has been suggested to account for relatively low Cl/B ratios in precipitation (Fogg and Duce, 1985).

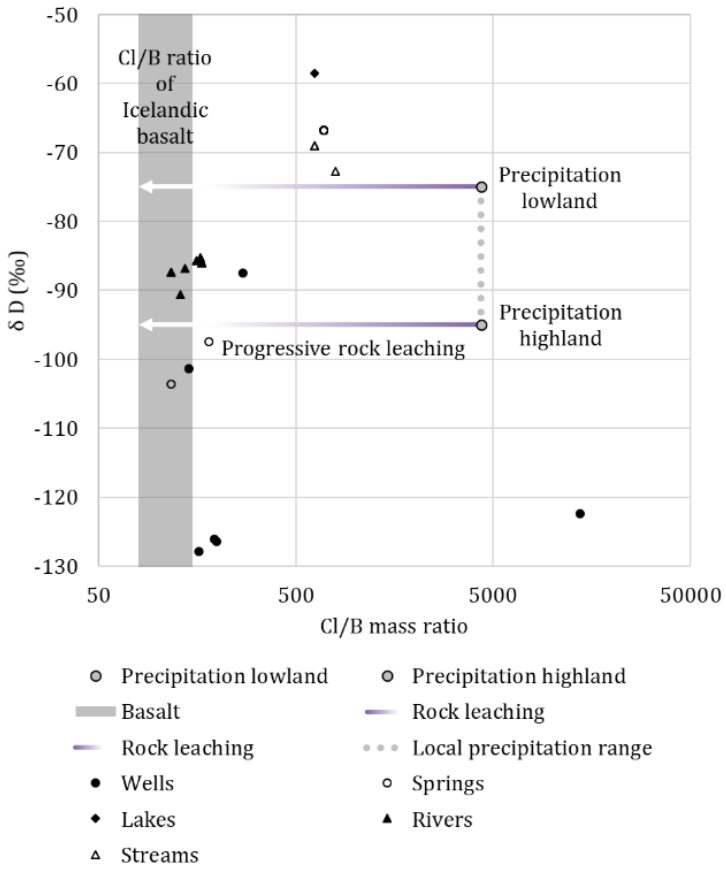

Figure 12. Relationship between the Cl/B mass ratio and δ^2H (δD) (‰) of the Húsavik-Hafralækur waters. The δ^2H values for the local precipitation (- 75 to – 95 ‰) (Árnason, 1976), and the progressive rock leaching towards the Cl/B rock ratio of average Icelandic basalts (80 - 150) (Arnórsson and Andrésdóttir, 1995) are shown as well. The Cl/B ratio for the local precipitation is the Cl/B seawater ratio (4 350) (Arnórsson, 1995). The figure shows that old, Ice Age waters (low δ^2H waters) are equilibrated with basalt.

5.4. Major elements and other parameters

In the same way as Cl and B, major elements are released from the rock to the water by water-rock interaction. The type of elements released to the water depend on the chemical composition of the rock as well as on the temperature at which water-rock interaction take place (Arnórsson et al., 1983).

Variations of the major elements and other parameters in the Húsavik-Hafralækur area with temperature are shown in Fig. 14, and maps of the geographical distribution of those parameters are found in Appendix B.

The results show that hot waters in the Húsavik-Hafralækur area have higher concentrations, and show covariations of Cl, B, SiO_2, Na, K, Al, SO_4, F and pH. This is an effect of water-rock interaction expected for low-temperature

geothermal waters that react with basalt (Kristmannsdóttir et al., 2010). This means that elevated concentrations of Cl, B, SiO_2, Na, K, Al, SO_4, F, and higher pH (> 9) are indicative of low-temperature geothermal waters originating from deeper aquifers in this area.

Cold waters show higher concentrations, and covariation of CO_2, Ca, Mg, Fe, and Sr. Higher concentrations of CO_2 can be indicative of water-rock interaction and/or mantle degassing, but in high-temperature geothermal areas (Stefánsson et al., 2017). A possible explanation for the CO_2 bearing cold waters in the Húsavik-Hafralækur area is that CO_2 has been transported with surface runoff from the high-temperature geothermal area in the NVZ. The elevated CO_2 values in the Laxá river support this hypothesis, since it has its recharge area in lake Mývatn in the NVZ (Fig. 15). Covariation of Ca, Mg, Sr, and Fe with CO_2 indicate that the same process accounts for the higher concentrations of these elements in this area. Elevated CO_2 levels are also found in cold waters that are not fed by the Laxá river, indicating more than one source for the CO_2. According to the CO_2 record from the Vostok ice core, CO_2 levels during the termination and later part of the last Ice Age were around 200 ppm (Barnola et al., 1987; Shackleton, 2000) compared to the present CO_2 levels, which are above 400 ppm (ESRL, 2019). Therefore, a speculation is that some of the CO_2 in young surface waters may originate from the atmosphere and reflect recent rising atmospheric CO_2 levels.

It can be concluded that elevated concentrations of CO_2, Ca, Mg, Fe and Sr, are indicative of waters originating from surface waters and shallow aquifers in this area. This is supported by higher δ^2H, and $\delta^{18}O$ values.

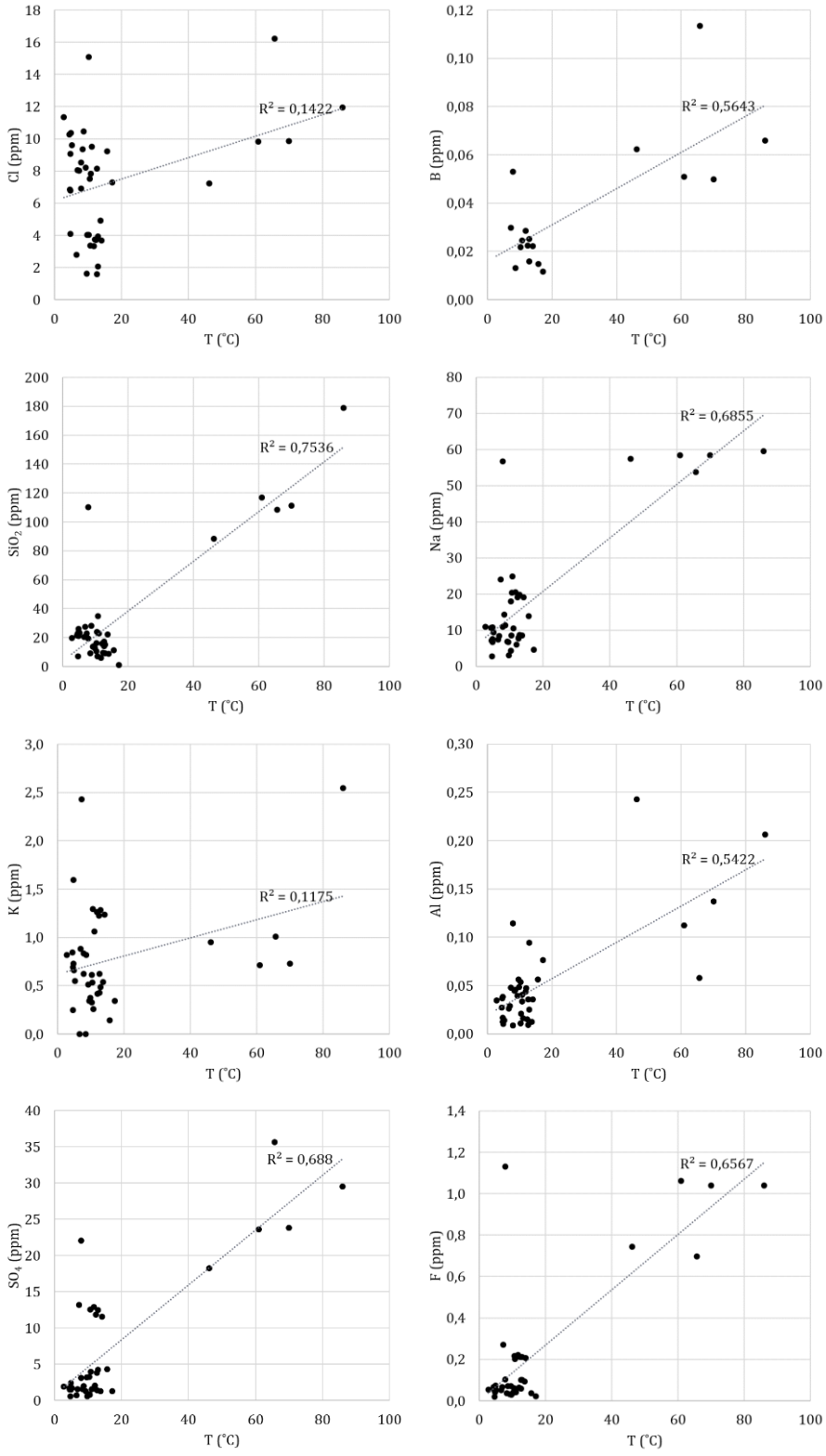
Cl (ppm)
R² = 0,1422
T (°C)
B (ppm)
R² = 0,5643
T (°C)
SiO2 (ppm)
R² = 0,7536
T (°C)
Na (ppm)
R² = 0,6855
T (°C)
K (ppm)
R² = 0,1175
T (°C)
Al (ppm)
R² = 0,5422
T (°C)
SO4 (ppm)
R² = 0,688
T (°C)
F (ppm)
R² = 0,6567
T (°C)

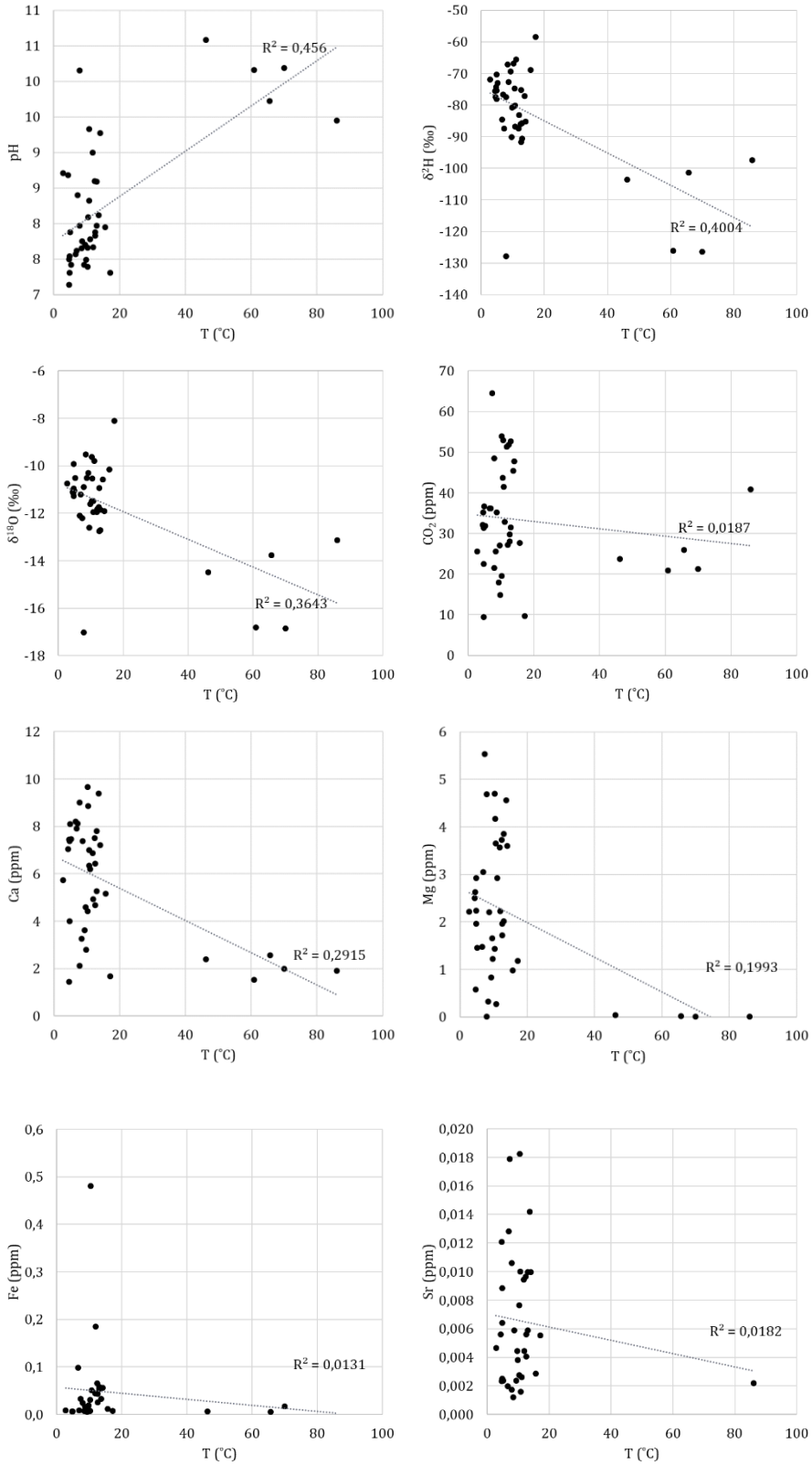

Figure 14. Bivariate plots of Cl, B, SiO_2, Na, K, Al, SO_4, F, pH, δ^2H, $\delta^{18}O$, CO_2, Ca, Mg, Fe, Sr and Temperature. Chloride, B, SiO_2, Na, K, Al, SO_4, F and pH covary and show increasing concentrations with rising temperature. δ^2H, $\delta^{18}O$, CO_2, Ca, Mg, Fe and Sr covary and show decreasing concentrations with rising temperature. Because of visual purposes, the extreme values at HU-01 are not included in the plots but would generally enhance the illustrated trends if they were so.

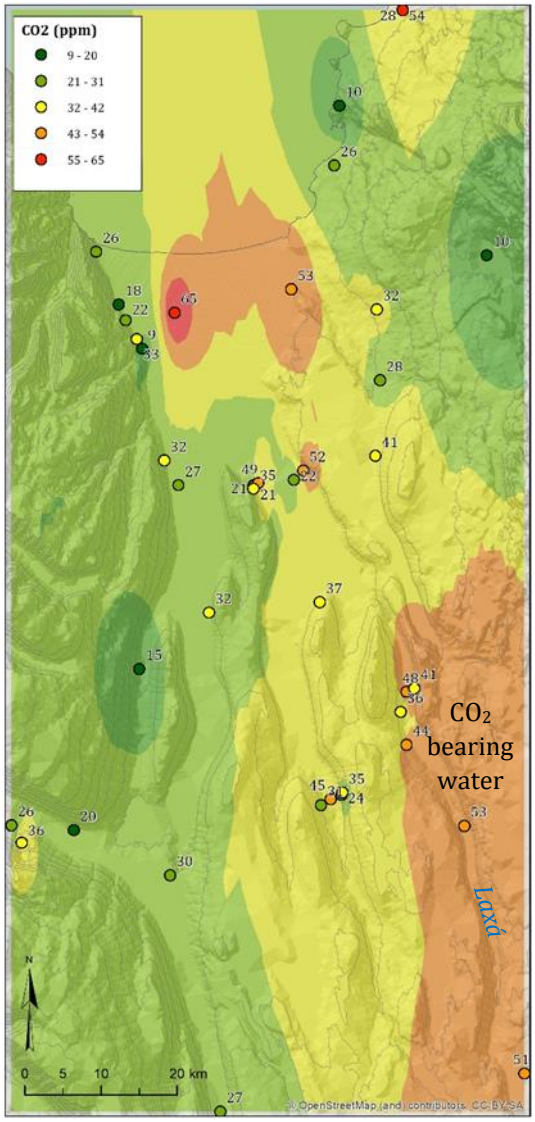

Figure 15. Map showing the distribution of CO_2 contents (ppm). The sample points and the measured values are shown on the map. The higher CO_2 content in the Laxá river indicates that CO_2 bearing water drains into the area as runoff from the NWZ.

5.5. Summary and hypothesis testing

This study shows that (1) modern meteoric waters are cold and are found at the surface and at shallow depths across the whole area; and (2) old Ice Age meteoric waters are mostly hot and are found at depth and at low altitudes close to the coast, where they ascend to the surface. These findings are in accordance with other studies in the Húsavik-Hafralækur area (Árnason, 1976), in the nearby areas Skagafjördur (e.g. Stefánsson et al., 2005) and Tröllaskagi (Ataş, 2006), as well as in other studies of natural waters in Iceland.

Hot waters are equilibrated with Icelandic basalt and show higher concentrations of Cl, B, SiO_2, Na, K, Al, SO_4 and F, as well as higher pH. Cold waters are less equilibrated with Icelandic basalt and show higher

concentrations of CO_2, Ca, Mg, Fe and Sr, as well as less negative δ^2H, and $\delta^{18}O$ values.

The waters in the Húsavik-Hafralækur area are meteoric. A seawater component is observed at the coast. Therefore, the hypothesis of a seawater gradient from the coast to the inland can be verified. There is also a δ^2H gradient from the coast inland which is consistent with but does not prove that there is a corresponding age gradient from the coast to the interior. Lack of evidence for closed system behaviour at the studied sites favours the hypothesis that Ice Age waters originate from an inland ice cap (Vatnjökull) as opposed to reflecting stagnation since an ice sheet covered the study area.

5.6. Conceptual hydrogeological model

A schematic conceptual hydrological model of the Húsavik-Hafralækur area is shown in Fig. 16. The model shows that the waters in the Húsavik-Hafralækur area are of meteoric origin and that there is a seawater gradient at the coast. Cold waters of modern age are found at all altitudes across the whole area at the surface and at shallow depths. Hot waters of pre-Holocene age are found in boreholes at low altitudes, close to sea level and near the coast, where they seem to rise to the surface in low permeable structures.

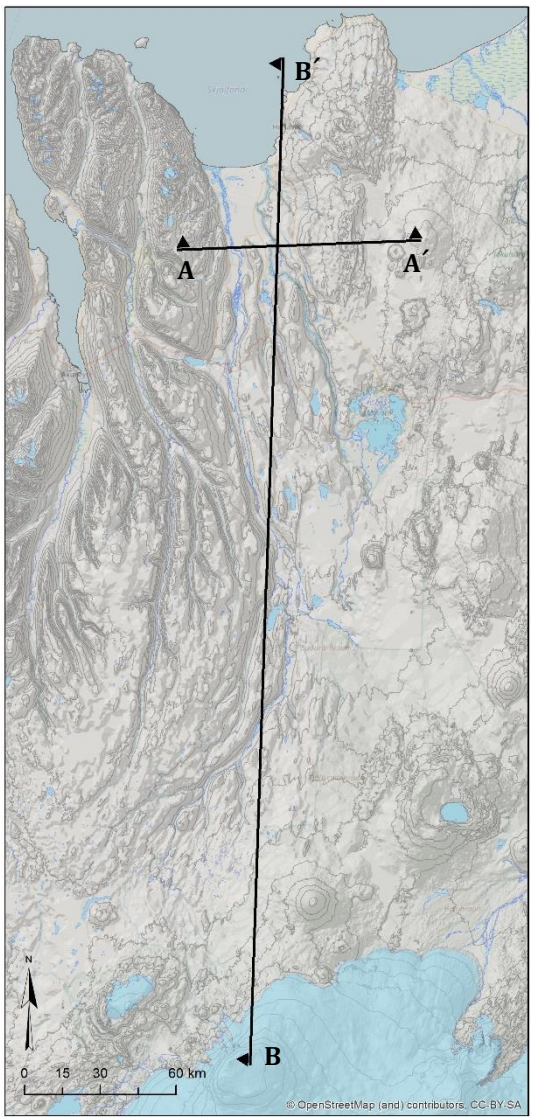

Figure 16. a) Map showing the locations of the hydrogeological cross sections A - A´ and B - B´ shown in Fig. 16 b and 16 c respectively.

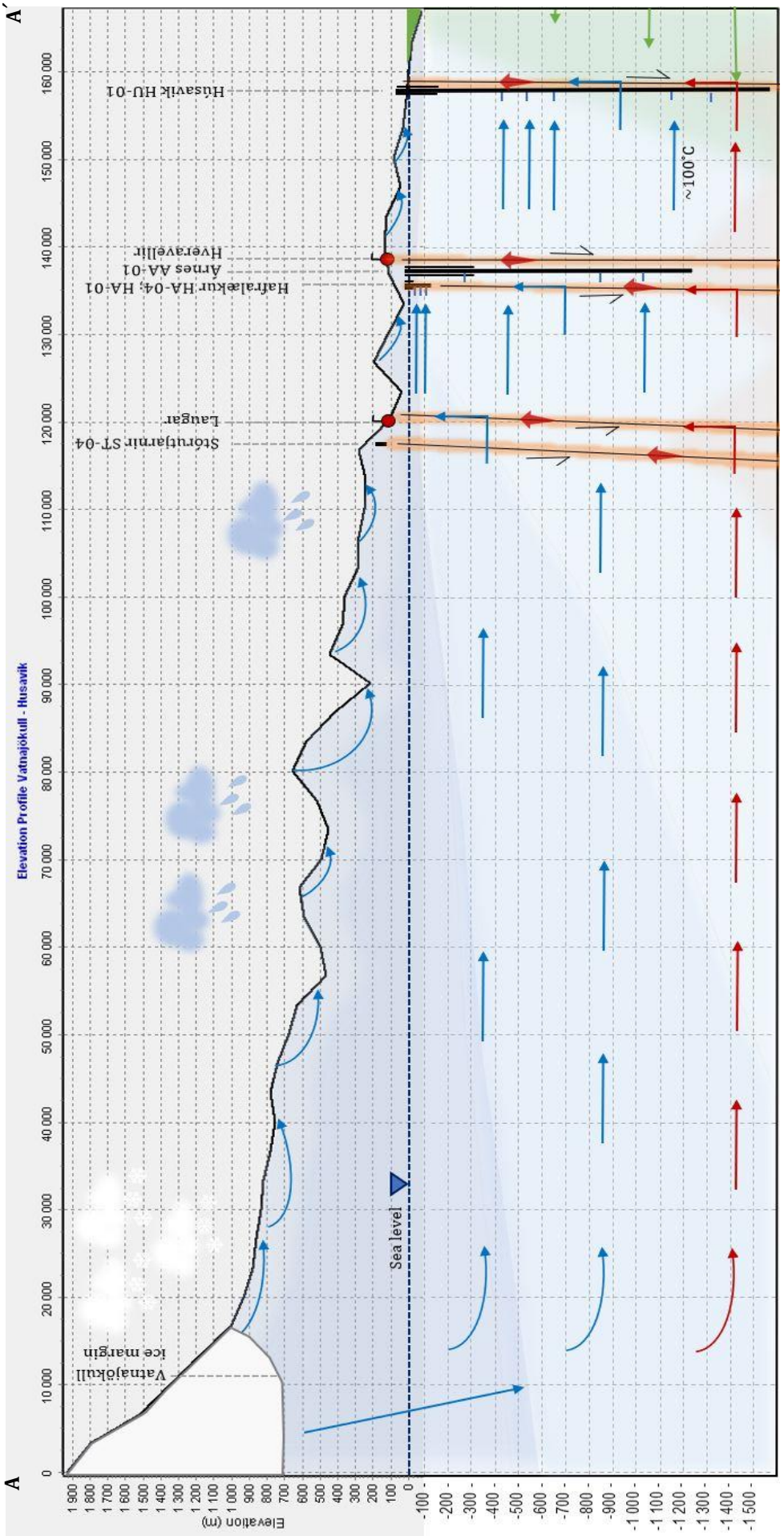

Figure 16. b) Cross section from A - A´ that shows a schematic conceptual hydrogeological model of the study area.

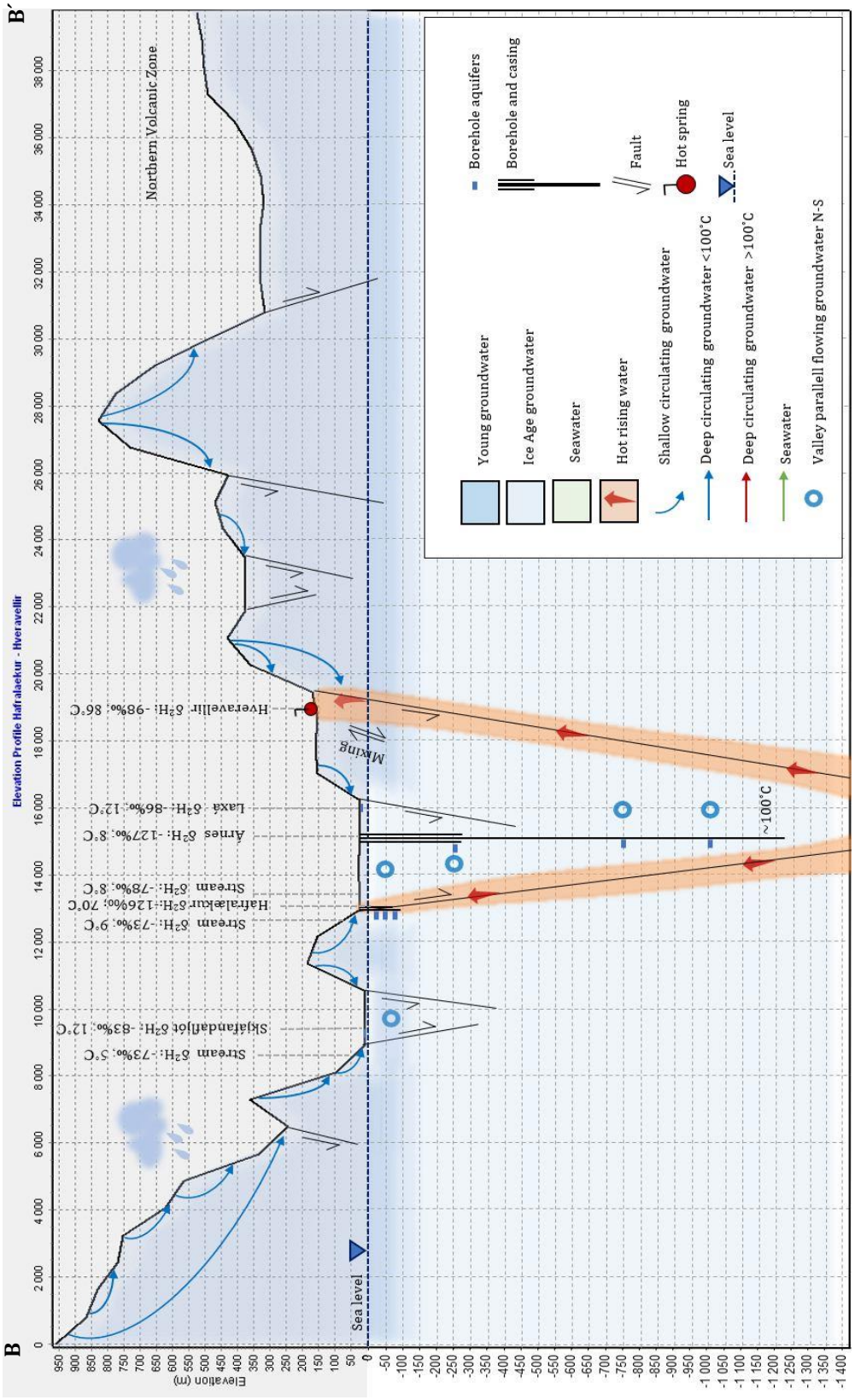

Figure 16. c) Cross section from B - B´ that shows a schematic conceptual hydrogeological model of the study area.

5.7. Implications

The results of this study show that the wells HU-01 and HA-01 are fed by Ice Age meteoric water that flows into the wells from below and/or from the side. HU-01 also receives a ~ 10 % seawater component that flows into the well from below and/or from the side. Modern meteoric waters are located in shallow aquifers above the Ice Age meteoric waters. Therefore, it is possible that mixing of these water sources may occur due to increased rock permeability caused by pre-seismic dilatational strain (Scholz et al., 1973). Since the aquifers are located so close, it is inferred that water mixing may be possible even at microscale fracturing, caused by very low pre-seismic dilatational strains (Skelton et al., 2019).

For both HU-01 and HA-01, an inflow of modern meteoric water from above may be associated with increases in δ^2H, and $\delta^{18}O$.

For HA-01, an inflow of modern meteoric water from above can also be associated with decreases in Cl, B, SiO_2, Na, K, Al, SO_4, F, and pH and increases in CO_2, Ca, Mg, Fe, and Sr. However, since CO_2, Ca, Mg, Fe, and Sr are associated with high-temperature alteration of basalt and mantle degassing (Arnórsson et al., 1983; Stefánsson et al., 2017), increases in those elements may also reflect an influx to the well from a deeper source.

For HU-01, the situation is more complicated due to the seawater component. However, due to the high concentration of dissolved solids at HU-01, an inflow of modern meteoric water from above may be associated with decreases in all major elements, but not CO_2.

At HA-01, the results of this study shows that an inflow of modern meteoric waters from above is probably responsible for the increases in δ^2H and $\delta^{18}O$, and may be responsible for the decreases in Cl, F and SO_4 documented before the 2012 and 2013 earthquakes (Skelton et al., 2019, 2014). The decreases of Cl, F and SO_4 could be explained by the CO_2 content added to the well by the modern meteoric water influx that maintained the charge balance by dissociation of $H_4SiO_4^0$ to $H_3SiO_4^-$ according to the speculation of Skelton et al. (2019).

The study supports the hypothesis that the second round of pre-seismic peaks at HA-01 (Si, Na, Ca, and Al), are caused by water-rock interaction (Skelton et al., 2014). This is because they covary. These peaks also show a lag compared to the δ^2H and $\delta^{18}O$ peaks, indicating that a different process account for these changes, supporting this hypothesis.

At HU-01, an inflow of any meteoric groundwater is unlikely to have caused the pre-seismic increases of Cu, Zn, Mn, Fe and Cr recorded for 2002 earthquake (Claesson et al., 2004), since the results show that meteoric waters only contain minor amounts of Fe (the other elements were not measured in this study). Instead, the results support the hypothesis that an inflow of a high-temperature fluid from a deep source below (possibly 4 – 6 km) caused the pre-seismic changes in Cu, Zn, Mn, Fe and Cr (Claesson et al., 2004).

The results support the hypothesis that the post-seismic decreases in δ^2H and $\delta^{18}O$ at HU-01 after the 2002 earthquake can be explained by a switch in the well from tapping one deep Ice Age aquifer to tapping another deep Ice Age

aquifer with even lower δ^2H values (Claesson et al., 2004). This inflow into the well may come from the side or from below. An inflow of modern meteoric water from above cannot explain these changes, since this would increase the δ^2H and $\delta^{18}O$ values, not lower them.

Whereas all the pre- and post-seismic hydrochemical changes at HA-01 can be explained with the dilatancy model (Scholz et al., 1973), the pre-seismic changes at HU-01 indicate an inflow of fluids rising from a deep mantle source, which is better explained by the model proposed by Stefánsson (2011).

5.8. Suggested further studies

Monitoring at HA-01 has shown coupling of hydrochemical changes with earthquakes (Andrén et al., 2016; Skelton et al., 2019, 2014). This study shows that two water sources are present at this site; an aquifer with Ice Age meteoric water (which also feeds the well) is located under an aquifer with modern meteoric water. This proximity can potentially enable mixing of these waters even by small increases in rock permeability. To extend the monitoring program with another well, a site with a similar hydrogeology is suggested to be targeted. This study shows that such conditions are found at Árnes. The AA-01 well taps an Ice Age aquifer located directly under an aquifer with modern water, which makes it a good candidate for future hydrochemical earthquake monitoring. The AA-01 well is flowing artesian, which excludes the risk of pump failures and incomplete records, and the road to the well makes it easily accessible all year round.

6. Conclusions

The groundwater in the Húsavik-Hafralækur area are of three hydrochemical types: modern meteoric water, pre-Holocene meteoric Ice Age water, and seawater.

Modern meteoric water constitutes surface waters and shallow aquifers over the whole area. Their characteristics are cold temperature, higher δ^2H and $\delta^{18}O$ values, and higher concentrations of CO_2, Ca, Mg, Fe and Sr.

Ice Age water constitutes deeper aquifers and emerges in lowland areas. Their characteristics are higher temperature, and higher concentrations of Cl, B, SiO_2, Na, K, Al, SO_4 and F, as well as higher pH, which reflects their equilibration with basalt. Ice Age waters may originate from a pre-Holocene ice cap located at Vatnajökull but could have stagnated from a pre-Holocene ice sheet located in the study area.

Seawater intruded at depth at the coast. Its characteristics are higher concentrations of Cl and other dissolved solids.

The HU-01 and HA-01 sites which have been used for studying coupling between earthquakes and changes of groundwater chemistry are fed by Ice Age waters that flow into the wells from below or from the sides, and the HU-01 also receives a ~ 10 % seawater component.

Since the study shows that there is only a short distance between the modern meteoric water source (above) and the Ice Age meteoric water source (below) at HA-01, it is inferred that water mixing may happen even at microscale fracturing, as an effect of pre-seismic dilatational strain (Scholz et al., 1973).

At HU-01, the hydrochemical situation is more complicated, since three water sources are present at the well site: modern meteoric water, Ice Age water, and seawater. The study supports that a fourth water component, originating from a high temperature mantle source, may have flown into the well prior to the 2002 earthquake. This influx may be associated with fluids rising from the mantle as an effect of plate rifting (Stefánsson, 2011).

Continued and extended hydrochemical earthquake monitoring in this area has great potential and can contribute to a deepened understanding of the earthquake evolution processes and improve the possibilities of future earthquake forecasting. This study shows that a promising site for extended earthquake monitoring is the AA-01 well at Árnes, and this well is suggested to be taken into the program for future monitoring.

Acknowledgements

I would like to thank my supervisor Alasdair Skelton for giving me the opportunity to do this fantastic project, as well as for professional guidance and support in all stages of the project. I would also like to thank Andri Stefánsson for being my supervisor, for all support and for organizing my training at Iceland University. I would like to thank Ríkey Kjartansdóttir for the training and analysis at Iceland University. I would like to thank Árný Sveinbjörnsdóttir, Hreinn Hjartarson, Gabrielle Stockmann, Erik Sturkell, and Barbara Kleine for guidance and help during fieldwork on Iceland. I would like to thank Arne Lif, Otto Hermelin, and Krister Junghahn for printing and binding my thesis and Elisabeth Däcker for the administration. I would like to thank my companion and friend Þrúður Helgadóttir for the amazing time on Iceland, the delicious Icelandic dinners and for being my private guide and teacher of Icelandic. It was so much fun. I would like to thank my husband Daniel for all support throughout this project and my whole education. Thank you all for making this project possible.

7. References

Andrén, M., Stockmann, G., Skelton, A., Sturkell, E., Mörth, C.-M., Guðrúnardóttir, H.R., Keller, N.S., Odling, N., Dahrén, B., Broman, C., Balic-Zunic, T., Hjartarson, H., Siegmund, H., Freund, F., Kockum, I., 2016. Coupling between mineral reactions, chemical changes in groundwater, and earthquakes in Iceland. J. Geophys. Res. Solid Earth 121, 2315–2337. https://doi.org/10.1002/2015JB012614

Andrés, N., Palacios, D., Saemundsson, Þ., Brynjólfsson, S., Fernández-Fernández, J.M., 2019. The rapid deglaciation of the Skagafjörður fjord, northern Iceland. Boreas 48, 92–106. https://doi.org/10.1111/bor.12341

Árnason, B., 1977. Hydrothermal systems in Iceland traced by deuterium. Geothermics 5, 125–151. https://doi.org/10.1016/0375-6505(77)90015-3

Árnason, B., 1976. Groundwater systems in Iceland traced by deuterium. Publ. Soc. Sci. Isl., 42, 236.

Arnórsson, S., 1995. Geothermal systems in Iceland: Structure and conceptual models—II. Low-temperature areas. Geothermics 24, 603–629. https://doi.org/10.1016/0375-6505(95)00026-7

Arnórsson, S., Andrésdóttir, A., 1995. Processes controlling the distribution of boron and chlorine in natural waters in Iceland. Geochim. Cosmochim. Acta 59, 4125–4146. https://doi.org/10.1016/0016-7037(95)00278-8

Arnórsson, S., Gunnlaugsson, E., Svavarsson, H., 1983. The chemistry of geothermal waters in Iceland. II. Mineral equilibria and independent variables controlling water compositions. Geochim. Cosmochim. Acta 47, 547–566. https://doi.org/10.1016/0016-7037(83)90277-6

Ataş, Ö.C., 2006. Geochemical and Isotopic Studies of Natural Waters from the Tröllaskagi Area, N-Iceland. Orkustofnun, Reports 2006, Nr. 6, Reykjavik.

Barnola, J.M., Raynaud, D., Korotkevich, Y.S., Lorius, C., 1987. Vostok ice core provides 160,000-year record of atmospheric CO 2. Nature 329, 408. https://doi.org/10.1038/329408a0

Björnsson, G., Hjartason, A., 2001. Hydrological monitoring stations in boreholes near the Husavik-Flatey fault zone. November 2000 to November 2001 performance. Orkustofnun. GrB-ArH-2001-05.

Bodvarsson, G., 1961. Physical charateristics of natural heat resources in Iceland. Jökull 29–38.

Chi-Yuen Wang, Manga, M., 2010. Hydrologic responses to earthquakes and a general metric. Geofluids 10, 206–216. https://doi.org/10.1111/j.1468-8123.2009.00270.x

Claesson, L., Skelton, A., Graham, C., Dietl, C., Mörth, M., Torssander, P., Kockum, I., 2004. Hydrogeochemical changes before and after a major earthquake. Geology 32, 641–644. https://doi.org/10.1130/G20542.1

Claesson, L., Skelton, A., Graham, C., Mörth, C.-M., 2007. The timescale and mechanisms of fault sealing and water-rock interaction after an earthquake. Geofluids 7, 427–440. https://doi.org/10.1111/j.1468-8123.2007.00197.x

Craig, H., 1961. Isotopic Variations in Meteoric Waters. Science 133, 1702–1703. https://doi.org/10.1126/science.133.3465.1702

Crampin, S., Volti, T., Chastin, S., Gudmundsson, A., Stefánsson, R., 2002. Indication of high pore-fluid pressures in a seismically-active fault zone. Geophys. J. Int. 151, F1–F5. https://doi.org/10.1046/j.1365-246X.2002.01830.x

Dobrovolsky, I.P., Zubkov, S.I., Miachkin, V.I., 1979. Estimation of the size of earthquake preparation zones. Pure Appl. Geophys. PAGEOPH 117, 1025–1044. https://doi.org/10.1007/BF00876083

Einarsson, P., Theodórsson, P., Hjartardóttir, Á., Guðjónsson, G., 2008. Radon Changes Associated with the Earthquake Sequence in June 2000 in the South Iceland Seismic Zone. Pure Appl. Geophys. 165, 63–74. https://doi.org/10.1007/s00024-007-0292-6

Einarsson, Þ., 1994. Geology of Iceland. Rocks and Landscape. Mál og menning, Reykjavik.

EPICA, community members, 2004. Eight glacial cycles from an Antarctic ice core | Nature. URL https://www.nature.com/articles/nature02599 (accessed 5.21.19).

ESRL, 2019. ESRL Global Monitoring Division - Global Greenhouse Gas Reference Network. URL https://www.esrl.noaa.gov/gmd/ccgg/trends/full.html (accessed 5.21.19).

Flovenz, O.G., Georgsson, L.S., Arnason, K., 1985. Resistivity structure of the upper crust in Iceland. J. Geophys. Res. 90, 10,136-10,150.

Fogg, T.R., Duce, R.A., 1985. Boron in the troposphere: Distribution and fluxes. J. Geophys. Res. Atmospheres 90, 3781–3796. https://doi.org/10.1029/JD090iD02p03781

Friðleifsson, G.Ó., 1997. Hafralækur, Hola 4. Orkustofnun, Greinargerð GÓF-97-01.

Friedman, I., Sigurgeirsson, T., Gardarsson, Ö., 1963. Deuterium in Iceland waters. Geochim. Cosmochim. Acta 27, 553–561. https://doi.org/10.1016/0016-7037(63)90012-7

Garcia, S., Dhont, D., 2005. Structural analysis of the Husavik-Flatey transform fault and its relationships with the rift system in Northern Iceland. Geodin. ACTA 18, 31–41.

Gudmundsson, A., Berg, S.S., Lyslo, K.B., Skurtveit, E., 2001. Fracture networks and fluid transport in active fault zones. J. Struct. Geol. 23, 343–353. https://doi.org/10.1016/S0191-8141(00)00100-0

Gudmundsson, A., Brynjolfsson, S., Jonsson, M.T., 1993. Structural analysis of a transform fault-rift zone junction in North Iceland. Tectonophysics 220, 205–221. https://doi.org/10.1016/0040-1951(93)90232-9

Hjartardóttir, Á.R., Einarsson, P., Bramham, E., Wright, T.J., 2012. The Krafla fissure swarm, Iceland, and its formation by rifting events. Bull. Volcanol. 74, 2139–2153. https://doi.org/10.1007/s00445-012-0659-0

Homberg, C., Bergerat, F., Angelier, J., Garcia, S., 2010. Fault interaction and stresses along broad oceanic transform zone: Tjörnes Fracture Zone, north Iceland. Tectonics 29. https://doi.org/10.1029/2008TC002415

Igarashi, G., Saeki, S., Takahata, N., Sumikawa, K., Tasaka, S., Sasaki, Y., Takahashi, M., Sano, Y., 1995. Ground-Water Radon Anomaly Before the Kobe Earthquake in Japan. Science 269, 60–61. https://doi.org/10.1126/science.269.5220.60

Ishikawa, T., Nakamura, E., 1992. Boron isotope geochemistry of the oceanic crust from DSDP/ODP Hole 504B. Geochim. Cosmochim. Acta 56, 1633–1639. https://doi.org/10.1016/0016-7037(92)90230-G

Jóhannesson, H., 2014. Geological Map of Iceland 1:600 000. Bedrock Geology. Icelandic Institute of Natural History, Reykjavik (2nd edition).

Jóhannesson, H., Sæmundsson, K., 2009. Geological Map of Iceland 1:600 000. Tectonics. Icelandic Insitute of Natural History, Reykjavik (1st edition).

Kissin, I.G., Grinevsky, A.O., 1990. Main features of hydrogeodynamic earthquake precursors. Tectonophysics 178, 277–286. https://doi.org/10.1016/0040-1951(90)90154-Z

Kristmannsdóttir, H., Arnórsson, S., Sveinbjörnsdóttir, Á., Ármannsson, H., 2010. Chemical Variety of Water in Icelandic Heating Systems. Proceedings World Geothermal Congress 2010. Bali, Indonesia, 25-29 April 2010.

Orme, L.C., Davies, S.J., Duller, G. a. T., 2015. Reconstructed centennial variability of Late Holocene storminess from Cors Fochno, Wales, UK. J. Quat. Sci. 30, 478–488. https://doi.org/10.1002/jqs.2792

Pope, E.C., Bird, D.K., Arnórsson, S., Giroud, N., 2016. Hydrogeology of the Krafla geothermal system, northeast Iceland. Geofluids 16, 175–197. https://doi.org/10.1111/gfl.12142

Reddy, D.V., Nagabhushanam, P., 2012. Chemical and isotopic seismic precursory signatures in deep groundwater: Cause and effect. Appl. Geochem. 27, 2348–2355. https://doi.org/10.1016/j.apgeochem.2012.08.023

Roeloffs, E.A., 1988. Hydrologic precursors to earthquakes: A review. Pure Appl. Geophys. 126, 177–209. https://doi.org/10.1007/BF00878996

Rögnvaldsson, S.T., Gudmundsson, A., Slunga, R., 1998. Seismotectonic analysis of the Tjörnes Fracture Zone, an active transform fault in north Iceland. J. Geophys. Res. Solid Earth 103, 30117–30129. https://doi.org/10.1029/98JB02789

Saemundsson, K., Frithleifsson, I.B., 1980. Application of geology in geothermal research in Iceland. Natturufraedingurinn 50, 157–188.

Sæmundsson, K., Stefánsson, V., Arnórsson, S., 1976. Jarðhitaborun í Árnesi, Aðaldal. Orkustofnun, Jadðhitadeild, OS JHD 7626.

Scholz, C.H., Sykes, L.R., Aggarwal, Y.P., 1973. Earthquake Prediction: A Physical Basis. Science 181, 803–810. https://doi.org/10.1126/science.181.4102.803

Seyfried, W.E., Janecky, D.R., Mottl, M.J., 1984. Alteration of the oceanic crust: Implications for geochemical cycles of lithium and boron. Geochim. Cosmochim. Acta 48, 557–569. https://doi.org/10.1016/0016-7037(84)90284-9

Shackleton, N.J., 2000. The 100,000-Year Ice-Age Cycle Identified and Found to Lag Temperature, Carbon Dioxide, and Orbital Eccentricity. Science 289, 1897–1902. https://doi.org/10.1126/science.289.5486.1897

Skelton, A., Andrén, M., Kristmannsdóttir, H., Stockmann, G., Mörth, C.-M., Sveinbjörnsdóttir, Á., Jónsson, S., Sturkell, E., Guðrúnardóttir, H.R., Hjartarson, H., Siegmund, H., Kockum, I., 2014. Changes in groundwater chemistry before two consecutive earthquakes in Iceland. Nat. Geosci. 7, 752–756. https://doi.org/10.1038/ngeo2250

Skelton, A., Liljedahl-Claesson, L., Wästeby, N., Andrén, M., Stockmann, G., Sturkell, E., Mörth, C.-M., Stefansson, A., Tollefsen, E., Siegmund, H., Keller, N., Kjartansdóttir, R., Hjartarson, H., Kockum, I., 2019. Hydrochemical Changes Before and After Earthquakes Based on Long-Term Measurements of Multiple Parameters at Two Sites in Northern Iceland—A Review. J. Geophys. Res. Solid Earth 0. https://doi.org/10.1029/2018JB016757

Stefánsson, A., Arnórsson, S., Sveinbjörnsdóttir, Á.E., 2005. Redox reactions and potentials in natural waters at disequilibrium. Chem. Geol. 221, 289–311. https://doi.org/10.1016/j.chemgeo.2005.06.003

Stefánsson, A., Hilton, D.R., Sveinbjörnsdóttir, Á.E., Torssander, P., Heinemeier, J., Barnes, J.D., Ono, S., Halldórsson, S.A., Fiebig, J., Arnórsson, S., 2017. Isotope systematics of Icelandic thermal fluids. J. Volcanol. Geotherm. Res. 337, 146–164. https://doi.org/10.1016/j.jvolgeores.2017.02.006

Stefánsson, R., 2011. Advances in Earthquake Prediction: Research and Risk Mitigation. Springer-Verlag, Berlin Heidelberg.

Stefánsson, R., Halldórsson, P., 1988. Strain release and strain build-up in the south Iceland seismic zone. Tectonophysics, Seismic Source Physics and Earthquake Prediction Research 152, 267–276. https://doi.org/10.1016/0040-1951(88)90052-2

Sveinbjörnsdóttir, Á.E., Johnsen, S.J., Arnórsson, S., 1995. The use of stable isotopes of oxygen and hydrogen in geothermal studies in Iceland. Proceedings of the World Geothermal Congress 1995, Florence, Italy, 1043–1048.

Thomas, D., 1988. Geochemical precursors to seismic activity. Pure Appl. Geophys. 126, 241–266. https://doi.org/10.1007/BF00878998

Thorsteinsson, T., Elíasson, J., 1970. Geohydrology of the laugarnes hydrothermal system in Reykjavik, Iceland. Geothermics, Proceedings of the United Nations symposium on the development and utilization of geothermal resources 2, 1191–1204. https://doi.org/10.1016/0375-6505(70)90432-3

Tómasson, J., Pálmason, G., Jónsson, J., Björnsson, S., 1969. Jarðhiti við Húsavík. Orkustofnun, Jadðhitadeild (Lithological report from the Icelandic Energy Association). Reykjavik, Iceland. 46 pp.

Tsunogai, U., Wakita, H., 1995. Precursory Chemical Changes in Ground Water: Kobe Earthquake, Japan. Science 269, 61–63. https://doi.org/10.1126/science.269.5220.61

Walker, G.P.L., 1960. Zeolite Zones and Dike Distribution in Relation to the Structure of the Basalts of Eastern Iceland. J. Geol. 68, 515–528.

Wang, B., Liu, Y., Sun, X., Ma, Y., Zhang, L., Ren, H., Fang, Z., 2018. Hydrogeological and Geochemical Observations for Earthquake Prediction Research in China: A Brief Overview. Pure Appl. Geophys. 175, 2541–2555. https://doi.org/10.1007/s00024-018-1885-y

Wästeby, N., Skelton, A., Tollefsen, E., Andrén, M., Stockmann, G., Claesson Liljedahl, L., Sturkell, E., Mörth, M., 2014. Hydrochemical monitoring, petrological observation, and geochemical modeling of fault healing after an earthquake. J. Geophys. Res. Solid Earth 119, 5727–5740. https://doi.org/10.1002/2013JB010715

Whitcomb, J.H., Garmany, J.D., Anderson, D.L., 1973. Earthquake Prediction: Variation of Seismic Velocities before the San Francisco Earthquake. Science 180, 632–635. https://doi.org/10.1126/science.180.4086.632

Appendix A

Complete list of chemical composition, Temperature and pH for the sampled waters in the Húsavik-Hafralækur area.

No.	Name	Site Location WGS84	Type	Temp °C	pH	Altitude m.a.s.l.	δ18O ‰	δD ‰	Cl mg/kg	B mg/kg	CO_2	SiO_2 mg/kg	Na mg/kg	K mg/kg	Ca mg/kg	Mg mg/kg	Fe mg/kg	Al mg/kg	SO_4 mg/kg	Sr mg/kg	Mn mg/kg	Br mg/kg	Mo mg/kg	Ti mg/kg	P mg/kg	Li mg/kg	F x̄ (ppm)		σ
1	Ljósavatn	N65°42.310', W017°39.922'	Lake	10	7,4	117	-11,5	-80	4,0	< 0.01	19,56	10	4	0,33	4,4	1,43	0,031	0,01	0,9	0,003	< 0.0125	< 0.075	< 0.005	< 0.0025	< 0.0175	< 0.005	0,038425	±	0,024695
2	Hafralækur HA-01	N65°52.351', W017°27.154'	Borehole	70	10,2	26	-16,8	-126	9,9	0,050	21,3	111	58	0,73	2,0	0,01	0,017	0,14	23,8								1,039845	±	0
3	Hafralækur HA-04	N65°52.332', W017°27.165'	Borehole	61	10,2	26	-16,8	-126	9,8	0,051	20,88	117	58	0,72	1,5	< 0.005	< 0.005	0,11	23,6								1,061896	±	0,020766
4	Árnes AA-01	N65°52.504', W017°24.325'	Borehole	8	10,2	32	-17,0	-128	8,5	0,053	21,56	110	57	0,62	2,1	0,01	< 0.005	0,11	22,0	0,002	< 0.0125	0,100	0,027	< 0.0025	< 0.0175	< 0.005	1,129799	±	0
5	Laxá by Árnes	N65°52.777', W017°23.658'	River	12	8,6	31	-11,7	-86	3,7	0,022	51,85	10	19	1,23	7,5	3,72	0,066	0,02	11,8	0,010	< 0.0125	< 0.075	< 0.005	< 0.0025	< 0.0175	< 0.005	0,212138	±	0,022757
6	Skjálfandafljót by Geirbjarnarstaðir	N65°52.345', W017°32.498'	River	12	7,7	11	-11,8	-83	3,7	< 0.01	27,14	16	6	0,42	4,9	2,22	0,185	0,05	2,1	0,004	0,013	< 0.075	< 0.005	0,004	< 0.0175	< 0.005	0,064217	±	0,048231
7	Þverá by Road 87	N65°55.388', W017°18.196'	Stream	13	7,8	106	-10,9	-75	8,1	< 0.01	28,03	17	8	0,63	6,4	1,96	0,044	0,01	1,5	0,006	< 0.0125	< 0.075	< 0.005	< 0.0025	< 0.0175	< 0.005	0,05823	±	0
8	Skjálfandafljót by Goðafoss	N65°40.992', W017°33.078'	River	13	7,9	125	-12,8	-92	1,6	< 0.01	29,73	14	8	0,43	4,7	1,72	0,026	0,04	3,9	0,004	< 0.0125	< 0.075	< 0.005	< 0.0025	< 0.0175	< 0.005	0,101	±	0,023618
9	Reykjadalsá by Laugar	N65°43.215', W017°21.713'	Stream	14	8,1	47	-10,6	-77	4,9	< 0.01	45,41	22	8	0,54	9,4	4,56	0,033	0,01	1,3	0,014	< 0.0125	< 0.075	< 0.005	< 0.0025	< 0.0175	< 0.005	0,094053	±	0
10	Laugar by Lautavegur	N65°43.040', W017°22.393'	Spring	5	7,5	98	-11,3	-78	6,8	< 0.01	31,36	24	7	0,73	7,4	2,92	< 0.005	0,01	1,8	0,006	< 0.0125	< 0.075	< 0.005	< 0.0025	0,032	< 0.005	0,058296	±	0,048446
11	Hafralækur stream by bridge	N65°52.404', W017°26.850'	Stream	8	8,0	31	-10,9	-78	6,9	< 0.01	48,52	19	11	0,83	9,0	4,69	0,024	0,01	3,2	0,011	< 0.0125	< 0.075	< 0.005	< 0.0025	< 0.0175	< 0.005	0,103385	±	0
12	Múlatorfa by Múli II	N65°48.949', W017°22.478'	Spring	5	7,9	112	-11,0	-75	10,4	< 0.01	36,72	26	11	0,66	8,1	2,24	0,006	0,01	2,4	0,003	< 0.0125	< 0.075	< 0.005	< 0.0025	0,052	< 0.005	0,074186	±	0,047909
13	Hveravellir by geyser	N65°53.200', W017°18.528'	Spring	86	9,5	148	-13,1	-97	11,9	0,066	40,85	179	60	2,55	1,9	0,01	< 0.005	0,21	29,6	0,002	< 0.0125	0,121	0,011	< 0.0025	< 0.0175	0,018	1,039845	±	0
14	Laxá by bridge	N65°58.023', W017°24.493'	River	13	8,6	9	-11,8	-86	3,9	0,025	52,69	9	20	1,28	7,8	3,85	0,054	0,03	12,5	0,010	< 0.0125	< 0.075	< 0.005	< 0.0025	0,023	< 0.005	0,212138	±	0,022757
15	South of Geirbjarnarstaðir	N65°53.068', W017°33.498'	Stream	5	7,4	48	-10,5	-73	9,6	< 0.01	31,9	23	9	0,55	7,5	1,45	< 0.005	0,01	1,7	0,002	< 0.0125	< 0.075	< 0.005	< 0.0025	0,030	< 0.005	0,051581	±	0,024372
16	Nípá River by Nípá farm	N65°56.305', W017°35.073'	River	5	7,1	11	-11,0	-74	4,1	< 0.01	9,41	7	3	0,25	1,4	0,58	< 0.005	0,02	0,6	0,002	< 0.0125	< 0.075	< 0.005	< 0.0025	< 0.0175	< 0.005	0,020034	±	0,025394
17	North of Núpá	N65°56.579', W017°35.452'	Spring	11	7,8	9	-9,8	-66	9,5	< 0.01	32,89	23	10	1,06	6,2	2,92	< 0.005	0,02	1,6	0,003	< 0.0125	< 0.075	< 0.005	< 0.0025	< 0.0175	< 0.005	0,040368	±	0,024641
18	Húsavík HU-01	N66°03.323', W017°21.086'	Borehole	98	9,0	69	-15,0	-122	1709,5	0,125	9,88	88	860	26,80	247,1	0,02	< 0.005	0,06	87,8								0,153846	±	0,023134
19	Halldórsstaðir	N65°44.797', W017°16.332'	Stream	11	8,1	179	-10,5	-75	7,5	< 0.01	43,71	24	9	0,53	8,9	4,17	0,481	0,02	0,8	0,018	0,018	< 0.075	< 0.005	< 0.0025	< 0.0175	< 0.005	0,06112	±	0
20	Above Skarðaborg	N65°57.445', W017°18.439'	Spring	4	8,7	138	-11,1	-75	10,3	< 0.01	32,04	21	11	0,85	7,1	2,50	< 0.005	0,03	1,7	0,006	< 0.0125	< 0.075	< 0.005	< 0.0025	0,037	< 0.005	0,06573	±	0,024103
21	Laxá by Sogsbrú	N65°46.339', W017°16.320'	River	14	9,3	132	-11,9	-85	3,7	0,022	47,71	9	19	1,23	7,2	3,60	0,056	0,04	11,6	0,010	< 0.0125	< 0.075	< 0.005	< 0.0025	0,033	< 0.005	0,207311	±	0
22	Hills east of Sogsbrú	N65°46.445', W017°15.778'	Spring	11	9,3	173	-11,5	-80	7,8	< 0.01	41,41	35	25	0,26	6,4	0,27	< 0.005	0,03	4,0	0,002	< 0.0125	< 0.075	< 0.005	< 0.0025	< 0.0175	< 0.005	0,202687	±	0,022811
23	Stóridalur by Stórutjarnir	N65°41.438', W017°43.612'	Spring	7	7,6	268	-12,1	-85	2,8	< 0.01	36,21	20	7	< 0.1	8,2	1,48	0,098	0,03	0,7	0,002	< 0.0125	< 0.075	< 0.005	< 0.0025	0,031	< 0.005	0,051581	±	0,024372
24	Stórutjarnir ST-04	N65°42.454', W017°44.342'	Borehole	66	9,7	177	-13,8	-101	16,2	0,114	25,9	108	54	1,01	2,6	0,01	0,006	0,06	35,6								0,697191	±	0,021304
25	Haukamýri	N66°01.602', W017°21.447'	Spring	3	8,7	33	-10,7	-72	11,3	< 0.01	25,56	20	11	0,82	5,7	2,22	0,009	0,03	1,9	0,005	< 0.0125	< 0.075	< 0.005	< 0.0025	0,045	< 0.005	0,052838	±	0
26	North of Halldórsstaðir	N65°45.756', W017°16.756'	Spring	7	7,6	163	-11,2	-77	8,0	< 0.01	36,17	28	8	0,88	7,9	3,05	0,009	0,03	1,6	0,013	< 0.0125	< 0.075	< 0.005	< 0.0025	0,032	< 0.005	0,06573	±	0,024103
27	Laxá by Ferjuhöfn	N65°42.433', W017°12.227'	River	11	8,3	151	-12,0	-87	3,4	0,025	52,91	7	20	1,29	7,0	3,65	0,051	0,04	12,5	0,010	< 0.0125	< 0.075	< 0.005	< 0.0025	0,033	< 0.005	0,216966	±	0
28	Laxá exiting Mývatn	N65°35.182', W017°07.980'	River	12	9,0	269	-11,9	-87	3,3	0,029	51,34	6	20	1,26	6,9	3,57	0,045	0,04	12,9	0,009	< 0.0125	< 0.075	< 0.005	< 0.0025	0,033	< 0.005	0,222006	±	0,022703
29	East of Laugar	N65°43.338', W017°20.926'	Spring	46	10,6	120	-14,5	-104	7,2	0,062	23,69	88	57	0,95	2,4	0,04	0,006	0,24	18,2								0,742963	±	0
30	East of Laugar	N65°43.404', W017°20.878'	Spring	5	7,5	137	-11,1	-77	6,8	< 0.01	35,19	23	7	0,69	7,5	2,62	< 0.005	0,04	1,5	0,012	< 0.0125	< 0.075	< 0.005	< 0.0025	0,027	< 0.005	0,049124	±	0,024425
31	West of Björg farm	N65°57.125', W017°36.228'	Spring	5	7,3	57	-9,9	-70	9,1	< 0.01	22,49	21	8	1,60	4,0	1,96	0,006	0,04	1,5	0,009	< 0.0125	< 0.075	< 0.005	< 0.0025	0,032	< 0.005	0,042405	±	0,024587
32	North of Björg	N65°57.587', W017°36.707'	Stream	9	7,4	8	-10,3	-69	8,2	< 0.01	17,93	14	7	0,51	3,6	0,83	0,005	0,04	1,3	0,002	< 0.0125	< 0.075	< 0.005	< 0.0025	0,028	< 0.005	0,03076	±	0,049842
33	North of Bjargakrókur	N65°59.114', W017.38.313'	Stream	8	7,7	3	-9,5	-67	9,3	< 0.01	25,52	9	14	< 0.1	3,3	0,32	0,007	0,04	1,6	0,001	< 0.0125	< 0.075	< 0.005	< 0.0025	0,024	< 0.005	0,035666	±	0
34	Skjálfandafljót by Sandhaugur	N65°35.071', W017°29.526'	River	10	7,7	185	-12,6	-90	1,6	< 0.01	27,1	14	7	0,34	4,6	1,66	0,014	0,06	3,2	0,004	< 0.0125	< 0.075	< 0.005	< 0.0025	0,022	< 0.005	0,072368	±	0,023995
35	Gljúfurá by Hlíð farm	N65°47.009, W017°35.254'	Stream	10	7,5	71	-11,6	-81	4,0	< 0.01	14,91	13	3	0,37	2,8	1,22	0,019	0,05	0,6	0,004	< 0.0125	< 0.075	< 0.005	< 0.0025	< 0.0175	< 0.005	0,028513	±	0,025017
36	West of Hafralækur	N65°52.251', W017°27.181'	Stream	9	7,8	39	-10,5	-73	10,5	0,013	35,18	28	11	0,82	7,4	2,20	0,016	0,05	2,0	0,006	< 0.0125	0,109	< 0.005	< 0.0025	< 0.0175	< 0.005	0,07071	±	0,048016
37	Berg BE-01	N65°57.345', W017°32.777'	Borehole	7	8,4	7	-12,2	-88	8,0	0,030	64,54	23	24	2,43	8,1	5,54	0,033	0,05	13,2	0,018	0,019	< 0.075	< 0.005	< 0.0025	0,136	< 0.005	0,271982	±	0
38	Kaldakvísl	N66°06.084', W017°16.601'	Stream	16	8,0	41	-10,2	-69	9,2	0,015	27,65	11	14	0,14	5,2	0,98	0,012	0,06	4,3	0,003	< 0.0125	< 0.075	< 0.005	< 0.0025	< 0.0175	< 0.005	0,037476	±	0
39	South of Kaldakvísl	N66°06.077', W017°16.611'	Spring	10	7,7	46	-9,6	-67	15,1	0,022	53,85	16	18	0,61	9,7	4,70	0,007	0,05	3,3	0,008	< 0.0125	< 0.075	< 0.005	< 0.0025	< 0.0175	< 0.005	0,041555	±	0,098158
40	Höskuldsvatn	N65°59.003', W017°10.638'	Lake	17	7,3	277	-8,1	-58	7,3	0,012	9,67	1	5	0,34	1,7	1,18	0,007	0,08	1,3	0,006	< 0.0125	< 0.075	< 0.005	< 0.0025	< 0.0175	< 0.005	0,021637	±	0,050594
41	Skjálfandafljót	N65°48.646', W017°30.340'	River	13	8,0	16	-12,7	-91	2,1	0,016	31,52459	15	9	0,48	5,3	2,02	0,058	0,09	4,2	0,006	< 0.0125	< 0.075	< 0.005	< 0.0025	0,025	< 0.005	0,101214	±	0,07075
	Detection limits								*1*	*0,01*		*0,1*	*0,25*	*0,1*		*0,005*	*0,005*	*0,0075*	*0,2*	*0,0005*	*0,0125*	*0,075*	*0,005*	*0,0025*	*0,0175*	*0,005*			

Appendix B

Geographical distribution maps of $\delta^{18}O$, $\delta^{2}H$, Cl, B, pH, CO_2, Ca, Mg, Sr, Fe, Al, K, SiO_2, and SO_4.

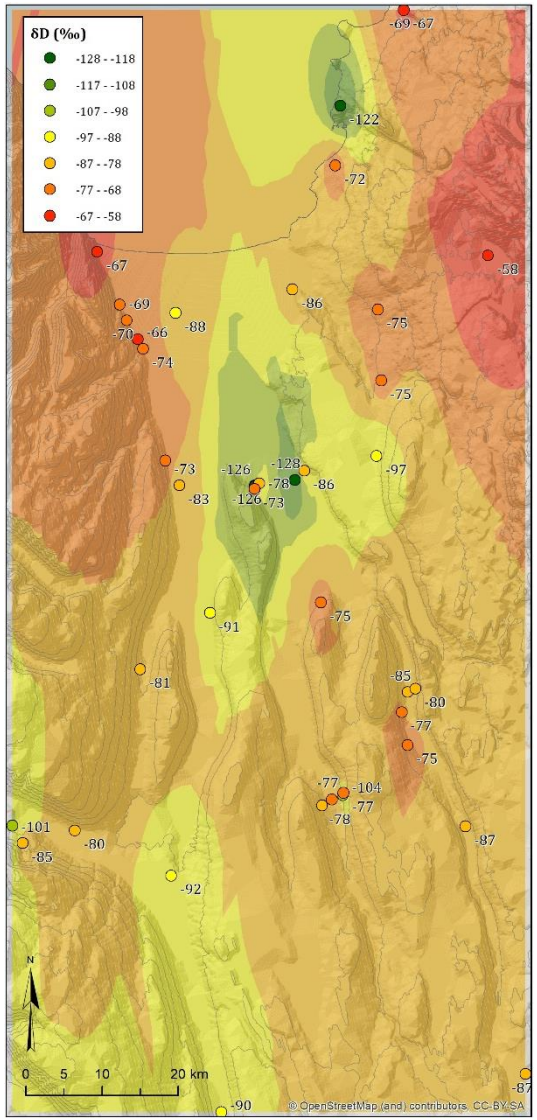

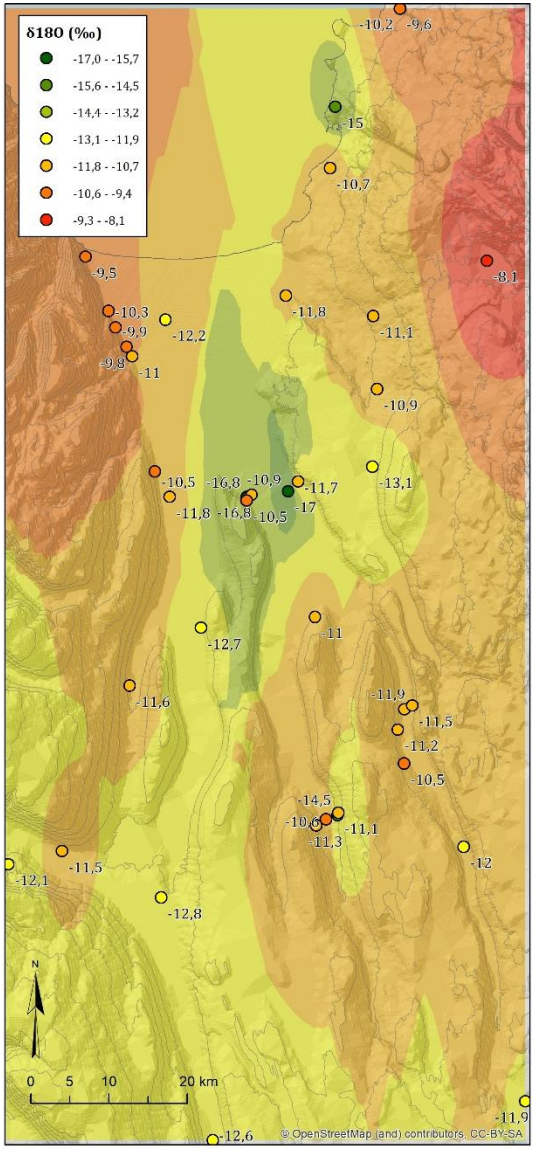

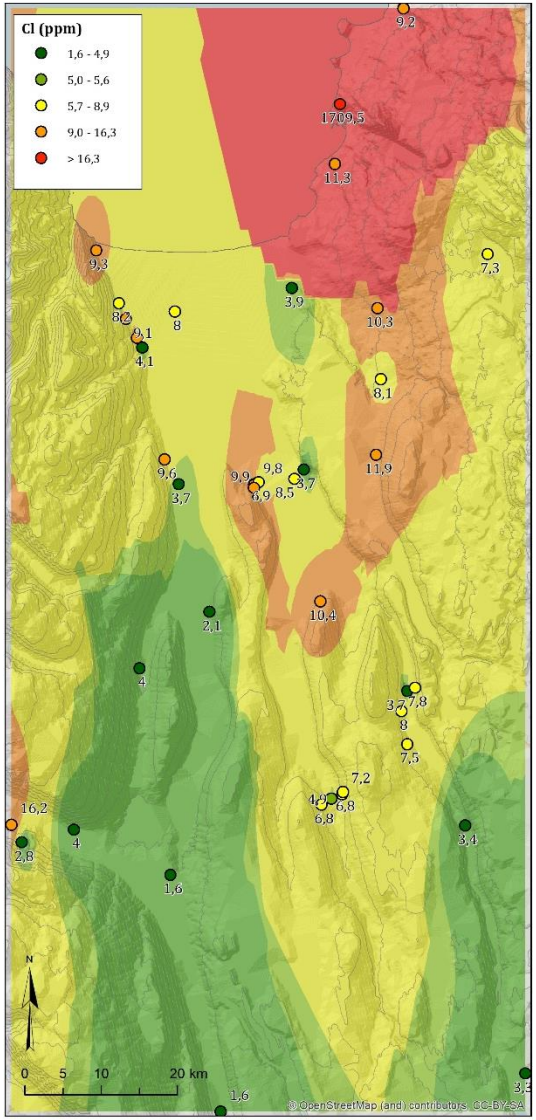
Cl (ppm)
1,6 - 4,9
5,0 - 5,6
5,7 - 8,9
9,0 - 16,3
> 16,3
9,2
1709,5
11,3
9,3
7,3
3,9
10,3
8,1
11,9
9,6
3,7
9,9
9,8
8,5
10,4
2,1
4
7,8
8
7,5
7,2
6,8
16,2
2,8
4
1,6
3,4
1,6
N
0 5 10 20 km
© OpenStreetMap (and) contributors, CC-BY-SA

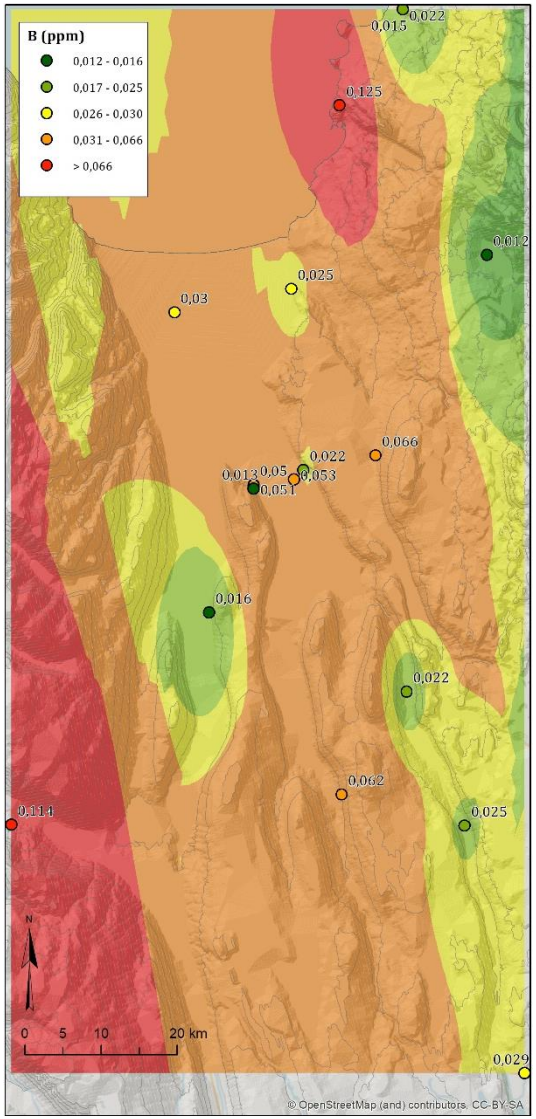
B (ppm)
0,012 - 0,016
0,017 - 0,025
0,026 - 0,030
0,031 - 0,066
> 0,066
0,022
0,015
0,125
0,012
0,025
0,03
0,066
0,022
0,013
0,05
0,053
0,051
0,016
0,022
0,062
0,114
0,025
0,029
N
0 5 10 20 km
© OpenStreetMap (and) contributors, CC-BY-SA

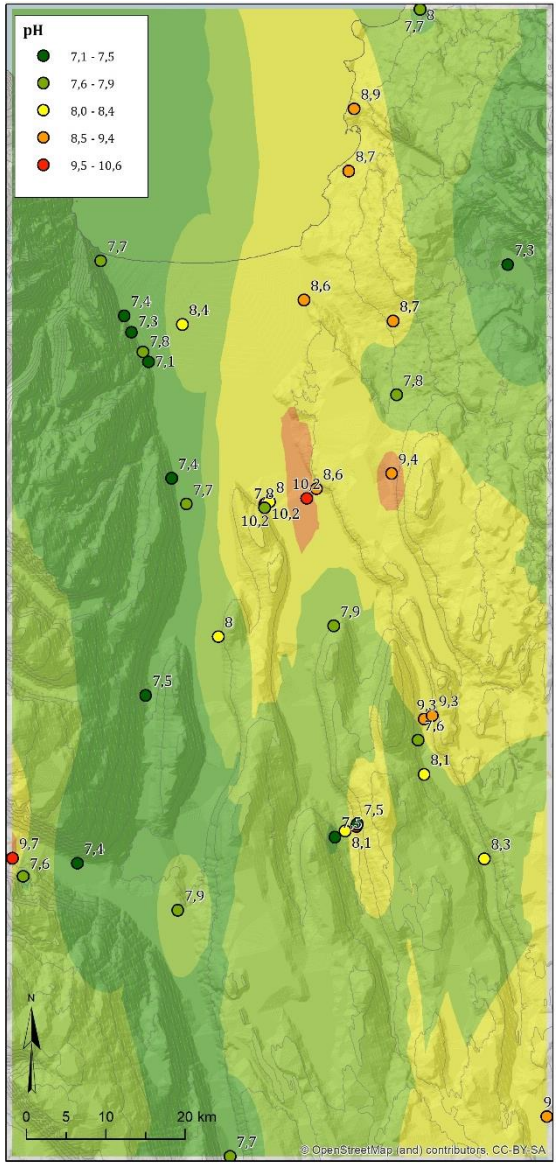
pH
7,1 - 7,5
7,6 - 7,9
8,0 - 8,4
8,5 - 9,4
9,5 - 10,6
0 5 10 20 km
© OpenStreetMap (and) contributors, CC-BY-SA

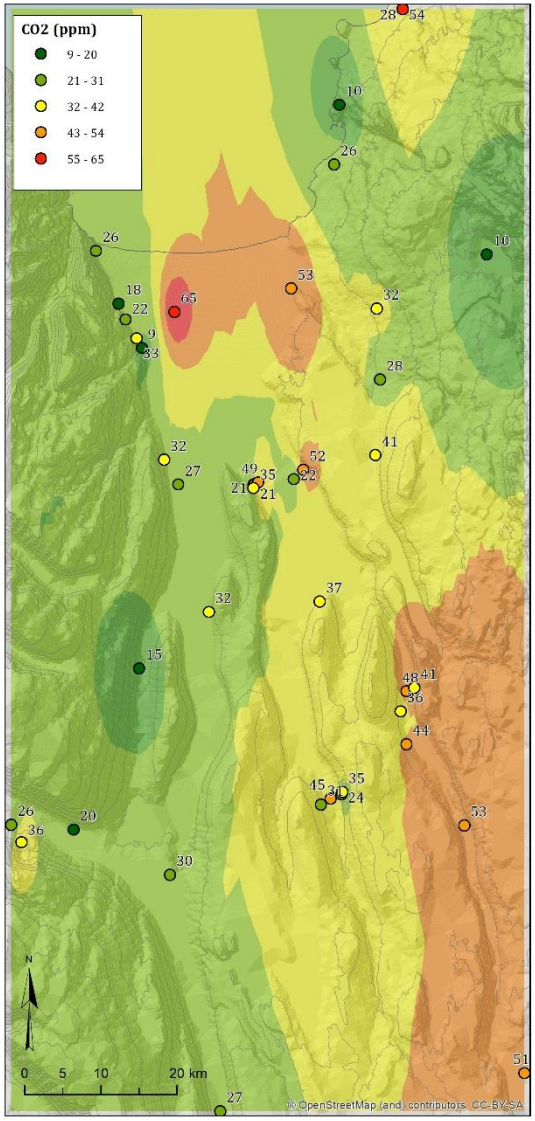
CO2 (ppm)
9 - 20
21 - 31
32 - 42
43 - 54
55 - 65
0 5 10 20 km
© OpenStreetMap (and) contributors, CC-BY-SA

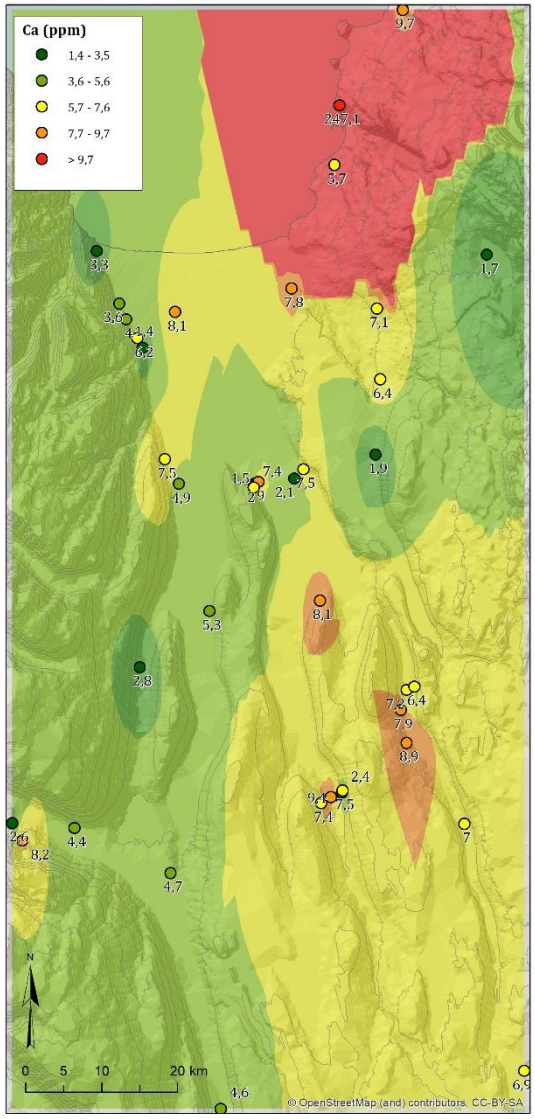
Ca (ppm)
1,4 - 3,5
3,6 - 5,6
5,7 - 7,6
7,7 - 9,7
> 9,7
0 5 10 20 km
© OpenStreetMap (and) contributors, CC-BY-SA

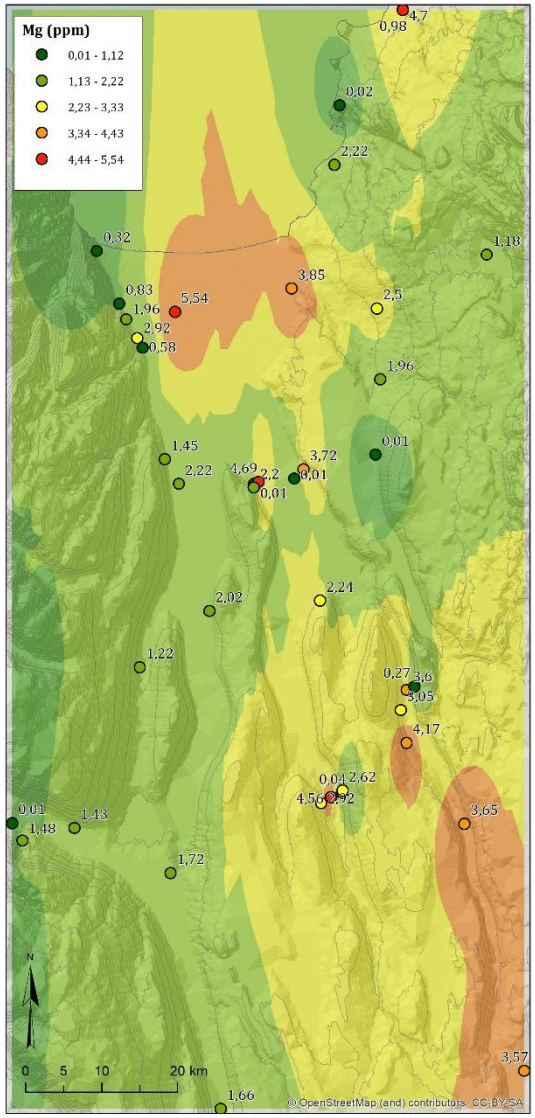
Mg (ppm)
0,01 - 1,12
1,13 - 2,22
2,23 - 3,33
3,34 - 4,43
4,44 - 5,54
0 5 10 20 km
© OpenStreetMap (and) contributors, CC-BY-SA

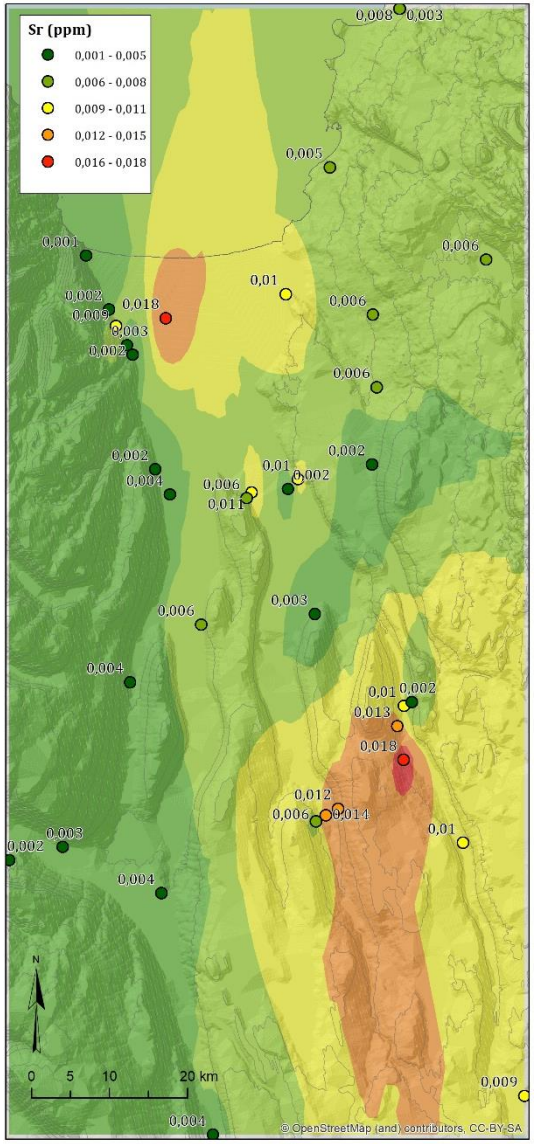
Sr (ppm)
0,001 - 0,005
0,006 - 0,008
0,009 - 0,011
0,012 - 0,015
0,016 - 0,018
0 5 10 20 km
© OpenStreetMap (and) contributors, CC-BY-SA

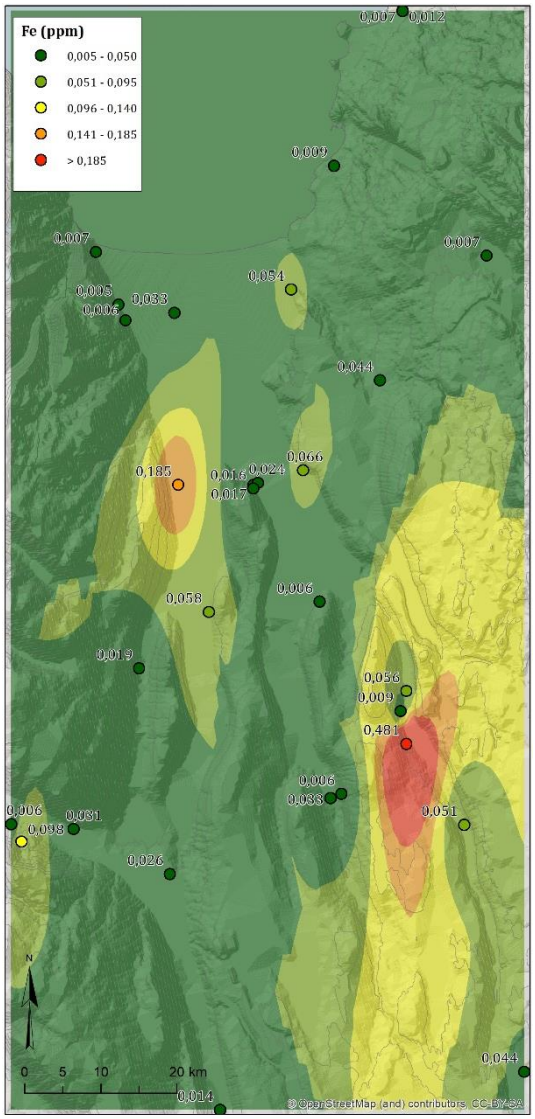
Fe (ppm)
0,005 - 0,050
0,051 - 0,095
0,096 - 0,140
0,141 - 0,185
> 0,185
0 5 10 20 km
© OpenStreetMap (and) contributors, CC-BY-SA

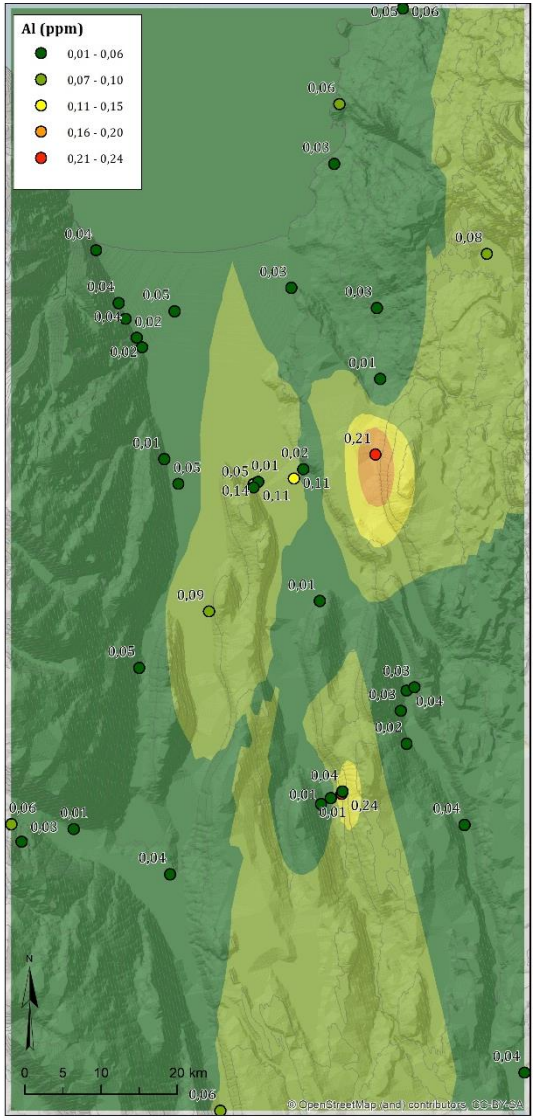
Al (ppm)
0,01 - 0,06
0,07 - 0,10
0,11 - 0,15
0,16 - 0,20
0,21 - 0,24
0 5 10 20 km
© OpenStreetMap (and) contributors, CC-BY-SA

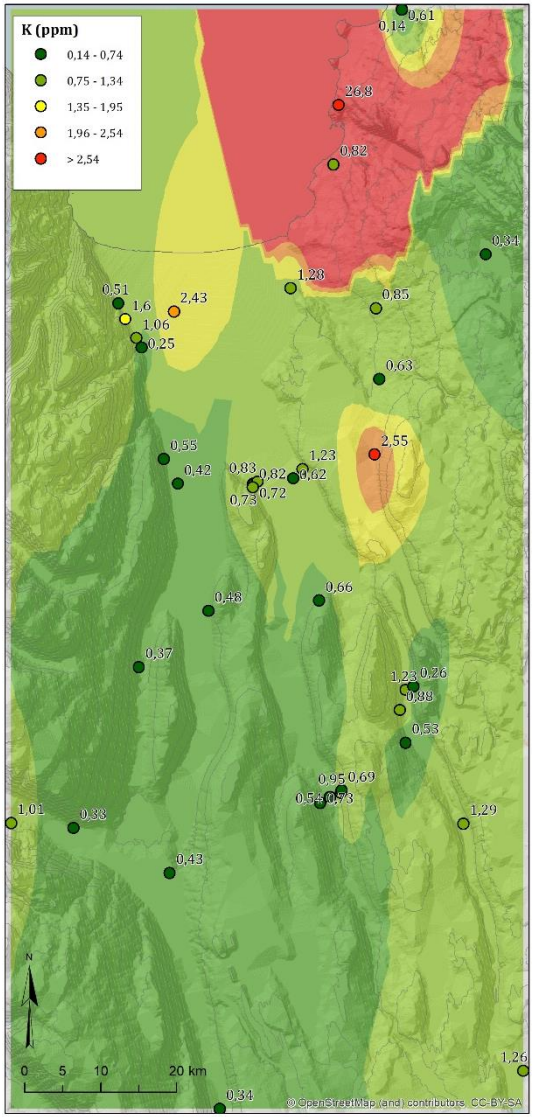
K (ppm)
0,14 - 0,74
0,75 - 1,34
1,35 - 1,95
1,96 - 2,54
> 2,54
0 5 10 20 km
© OpenStreetMap (and) contributors, CC-BY-SA

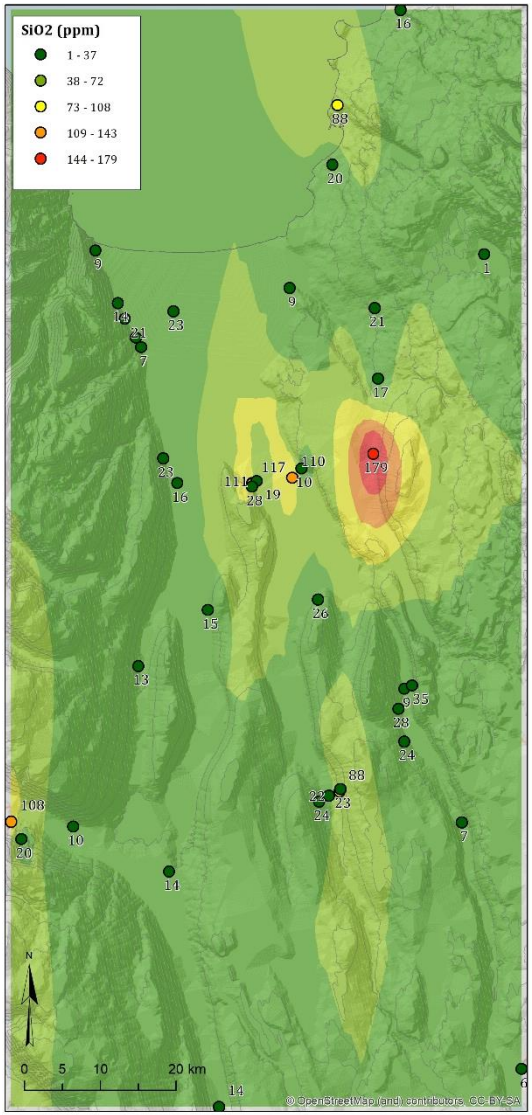
SiO2 (ppm)
1 - 37
38 - 72
73 - 108
109 - 143
144 - 179
0 5 10 20 km
© OpenStreetMap and contributors, CC-BY-SA

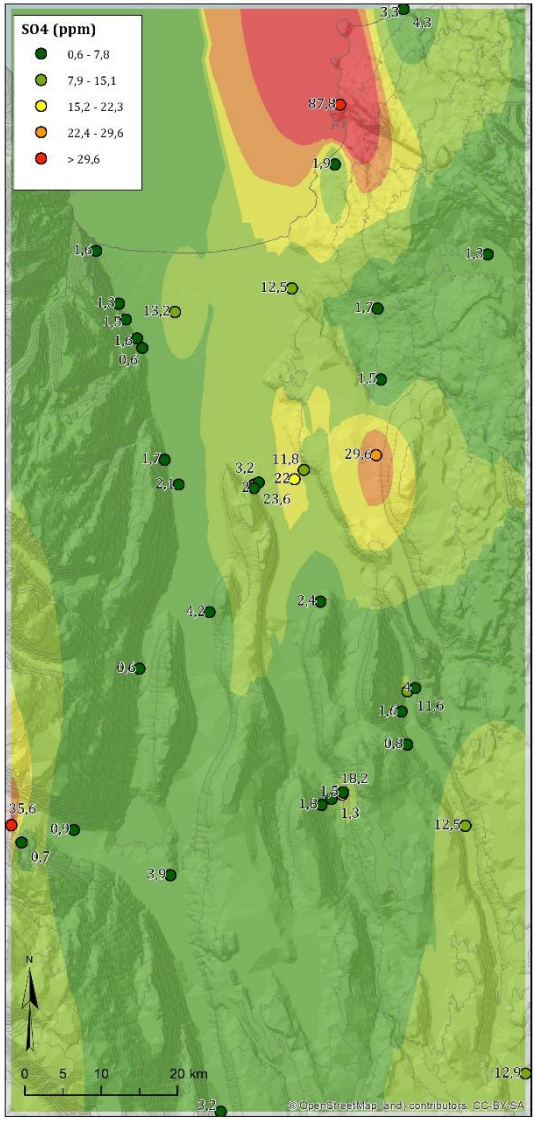
SO4 (ppm)
0,6 - 7,8
7,9 - 15,1
15,2 - 22,3
22,4 - 29,6
> 29,6
0 5 10 20 km
© OpenStreetMap and contributors, CC-BY-SA